#### 2.3.1.3 All Hadronic Mode

We have found a clear signal in the all-hadronic decay channel for $t\bar{t}$ events. In this decay mode there are six final state jets, four of which come from the hadronic decays of the two W's and two from the $b$-quarks. Approximately 44% of $t\bar{t}$ events have this decay signature. Achieving a reasonable signal-to-background ratio is the challenge in this data set which is dominated by QCD multijet production. In order to isolate a signal and maintain efficiency, we require at least five well-separated jets, one of which must be SVX $b$-tagged. After additional topological cuts, we find 222 tags in 187 events with an estimated background of 151 $\pm$ 10 events. Figure 2.14 (lower left) shows the jet multiplicity spectrum for the all-hadronic channel. In the 4-jet bin where we expect little contribution from $t\bar{t}$ events, the background and observed tags are in good agreement(12 observed vs 11.7 expected). Where we expect to see a signal for $t\bar{t}$, in the 5, 6, and $\geq$7-jet bins, an excess of tags is observed over the background predictions. [8]

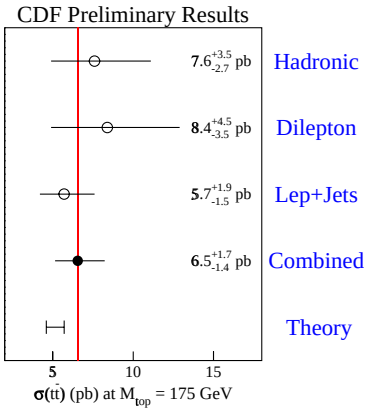


Figure 2.15: The measured cross section for $t\bar{t}$ production for each of the separate production channels measured at CDF as well as our combined measurement. The vertical line represents our average value. The bottom most point is an indication of the current theoretical calculations evaluated at a top mass of 175 GeV/$c^2$.

#### 2.3.1.4 Kinematic Discrimination

In addition to the search techniques based on the dileptons and $b$-quark tagging, CDF has isolated $t\bar{t}$ events based on the kinematical properties predicted from Monte Carlo simulations. These methods use the lepton+jets event sample but do not rely on $b$-tagging to reduce the background. One technique examines the jet $E_T$ spectra of the second and third highest $E_T$ jets [5]. The second technique uses the total transverse energy of the event [6]. In both cases, there is a clear $t\bar{t}$ component in our data.

#### 2.3.1.5 $t\bar{t}$ Production Cross Section

The counting experiments which lead to a confirmed signal can be turned directly into measurements of the $t\bar{t}$ production rate. Figure 2.15 shows the $t\bar{t}$ production cross section measured in several channels in comparison to recent theoretical predictions. Our best measurement is obtained from the weighted average of the counting experiments performed in the dilepton channel, the two lepton+jets channels, SVX $b$-tagging and SLT $b$-tagging, and the all-hadronic channel. With 105 pb$^{-1}$ of data, we measure a production cross section by combining the measurements in each of the separate channels to be $6.5^{+1.7}_{-1.4}$ pb[36, 37]. The production cross section in the individual decay channels are found to be $5.7^{+1.9}_{-1.5}$ pb for the Lepton+jets mode [36], $8.4^{+4.5}_{-3.5}$ pb for the dilepton mode [38], and $7.6^{+3.5}_{-2.7}$ pb for the hadronic mode [39]. A theoretical cross section calculation by Mangano *et al.* predicts 5.2 pb[18] at 175 GeV/c$^2$, and other recent theoretical cross sections are within approximately 10% of this value.[18, 19]

#### 2.3.1.6 Top Quark Mass

The top quark mass has been measured in three different channels. The primary method is based on fully reconstructing the $t\bar{t}$ system with lepton+jets events. These events must contain a lepton and at least four jets such that each final state parton can be assigned to an observed jet or lepton. The reconstruction is performed using a constrained fitting technique which selects the best assignment of observed jets to final state partons based on the lowest $\chi^2$. Without any $b$-tagging information there are 24 combinations which must be considered (12 parton assignments $\times$ 2 possible longitudinal momentum components for the neutrino). When one or two jets are tagged as $b$-quarks, the number of combinations is reduced to 12 and 4, respectively. In order to make the best use

of the data sets for measuring the top quark mass, the lepton+jets sample is divided into four orthogonal subsamples based on b-tagging: the SVX single-tagged set, the SVX double-tagged set, the SLT-only tagged set, and the not-tagged set [13]. The backgrounds are determined separately for each subset. The mass is determined by combining the likelihood functions defined in each subsample to extract a single optimized measurement of the top quark mass. This method currently yields the world's best top mass measurement of $176.1 \pm 5.1$ (stat.) $\pm 5.3$ (syst.) GeV/c$^2$[3] (see Figure 2.16). The systematic uncertainty is dominated by the uncertainty in final state gluon radiation and the detector energy scale.

The same constrained fitting technique was also used to reconstruct the top mass in the all-hadronic channel where at least one $b$-tag was required; the result is seen in Figure 2.14 (lower right). Applying a maximum likelihood technique to the data in this channel results in a top mass of $186 \pm 10$ (stat.) $\pm 5.7$ (syst.) GeV/c$^2$.

Reconstructing a top mass in the dilepton channel is difficult because this system is underconstrained due to the two undetected neutrinos. To solve this problem, we scan the two neutrinos and top mass to determine a probability function. Given the top mass, W mass, $\eta_{\nu_1}$, $\eta_{\nu_2}$, the two $b$ jets, and two leptons, one can solve for the top mass independently and compare the predicted missing energy with the measured as a weight estimator. This technique gives a top mass from dileptons of $167.4 \pm 10.3$ (stat.) $\pm 4.8$ (syst.) GeV/c$^2$.

In the subsample of lepton+$\geq$ 4-jet events where two $b$-tags are required, we have looked for evidence of the decay of the hadronic W-boson. Fig. 2.17 shows the reconstructed mass of the unconstrained jet-jet system. A fit yields a jet-jet mass of 79.8 $\pm$ 6.2 GeV/c$^2$ [15]. This will be an important *in situ* technique for jet energy scale calibration in Run II. The top mass from this double $b$-tagged subsample has been determined to be $174.8 \pm 8$ (stat.) $\pm 6$ (syst.) GeV/c$^2$.[14]

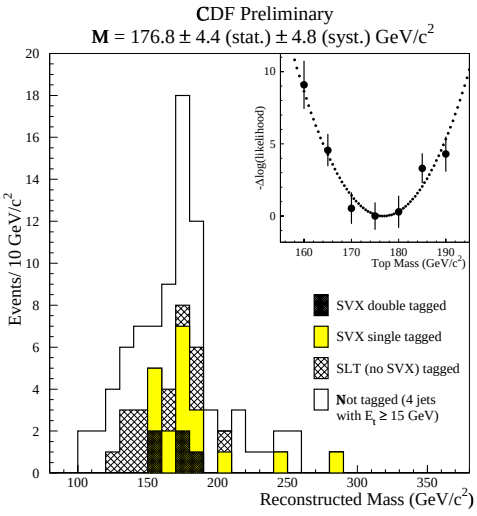


Figure 2.16: The optimized lepton+jets top quark mass plot for each of the four data samples. The light shaded area is the background expectation. The darker shaded region is the shape of the background + top expected for a top mass of 175 GeV/$^2$.The insert in each plot shows the -$\Delta$log(likelihood) for the data in comparison to mass spectra derived from Monte Carlo samples of various $m_{top}$ for that particular set of selection cuts. This technique results in a measured top quark mass of $176.1 \pm 5.1$ (stat.) $\pm 5.3$ (syst.) GeV/c$^2$.

### 2.3.2 Lessons from Run I

- The detector should have the greatest possible acceptance for high-$p_T$ electrons and muons from the chain $t \to W \to l\nu$.

- The detector should have the greatest possible acceptance and efficiency for tagging $b$-jets. This is a question of geometrical coverage, efficiency, and signal-to-noise ratio, most importantly for secondary vertex finding but also for soft lepton identification.

- Precision measurement of the top mass requires that the detector have *in situ* capability for understanding the systematics of jet energy calibration, including the ability to accumulate large samples triggered on low-$p_T$ charged tracks, inclusive photons, and inclusive $W \to l\nu$ and $Z \to ll$.

- Understanding of $b$-tagging systematics has relied on the ability to accumulate a large, reasonably pure control sample of inclusive $b$-jets using low-$p_T$ inclusive lepton triggers. We anticipate doing this again, with some demand on DAQ bandwidth. However, we have learned that jets containing $b \to cl\nu_l X$ are a biased control sample, and we believe that a large sample of $b$-

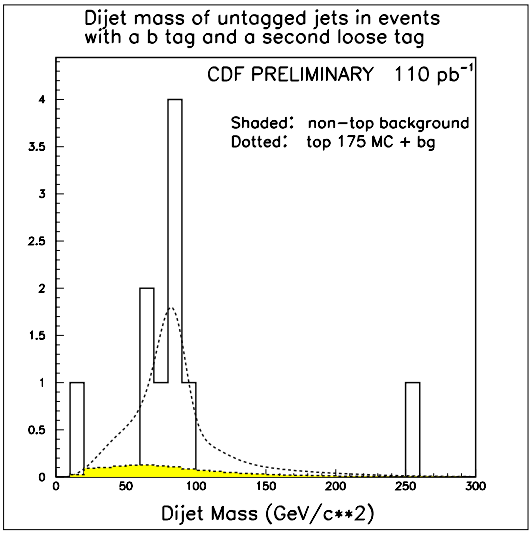


Figure 2.17: The $M_{jj}^W$ distribution is shown for data (solid), expected top+background (dashed), and background (shaded), for W+4 jet events which contain two $b$-tagged jets. The value of $M_{jj}^W$ is 79.8 $\pm$ 6.2 GeV/c$^2$. The top mass from this subsample has been determined to be 174.8 $\pm$ 9.7 GeV/c$^2$.

jets collected with a secondary vertex trigger will be extremely useful.

### 2.3.3 Impact of Upgrades on Top Physics

The impact of the CDF IIb upgrades is to maintain the significant increases in overall top acceptance that will be achieved in Run IIa and to maintain that increased acceptance and precision at high luminosity and maintain the precision for large integrated luminosity.

- **Silicon Vertex Detector (SVX IIb)**: SVXII was not built to survive the radiation levels that it would be exposed to for Run IIb. Layer 00 as well as the three innermost layers of SVXII need to be replaced in order to complete Run IIb with reasonable detector performance and thus meet our physics goals. Time constraints on the length of the Run IIa to IIb shutdown require that all of SVXII be replaced. The goal of the replacement device is to have comparable performance to SVXII - the one now in place for Run IIa. Since SVXII is still being commissioned, comparisons will be made between the Run I silicon and the proposed SVXII replacement.

  In top physics, the name of the game is acceptance and purity. The tagging of $b$-quarks from top quark decays will be greatly improved in the long, 7-layer device from what was used in run I. Increasing the length of the silicon from 52 cm to 96 cm will extend the region of "contained $b$-jets" to cover the entire interaction region. With seven measurements in two views for any given track, it will be possible to make stringent track quality requirements, reducing the level of mistags, while still improving the overall track finding efficiency.

  Taking all of these factors into account, we anticipate that the SVX II replacement will increase the efficiency for tagging at least one $b$-jet in a $t\bar{t}$ event to better than 65% (a 60% increase over the Run 1 efficiency), and will raise the double $b$-tag efficiency to 20% (a 200% increase from Run I performance) [23].

  Finally we point out that the 3D capability of the the new silicon detector will allow a precision measurement of the primary vertex in the event, improving a variety of measurements including the $E_t/P_t$ of the primary leptons, the $E_t$ of the jets, and the missing transverse energy.

- **Central Outer Tracker (COT) Upgrade**: The top analysis of Run I depended crucially on the large central tracking chamber. Similarly, the success of Run IIa top analysis will depend upon the performance of the Central Outer Tracker (COT). As luminosities increase for Run IIB, the inner superlayers of the COT will become less effective due to an increase in occupancy. Although track finding utilizing the outer superlayers will still be possible, the ability to point back to the silicon will be degraded due to low hit usage on the inner superlayers. On complicated events such as those found in $t\bar{t}$, this effect would be extremely detrimental to our ability to reconstruct the event properly. Thus deadening the sense wires at large $|\eta|$ would give back most of the fine performance expected in the Run IIA COT.

- **Muon Detection System**: In the Run I top analysis, only "central" muons were used as the primary lepton - that is those muons which were detected in the region covered by the CMU and CMP detectors. Muons that passed through the

| Channel | Acc. $A_{IB}$ (Run Ib) | Acc.,$A_{II}$ (Run IIb) | Run I Results | Run IIb Yield (w/ $A_{II}$) |
|---|---|---|---|---|
| Produced $t\bar{t}$ | - | - | 525 | 100k |
| Dileptons ($ee$,$\mu\mu$,$e\mu$) | 0.78% | 1.1% | 10 | 1200 |
| Tau dileptons ($e\tau$, $\mu\tau$) | 0.12% | 0.14% | 4 | 142 |
| lepton+$\geq$3j | 9.2% | 11.2% | 324 | 10000 |
| lepton+$\geq$3j w/ $\geq$1 $b$ tag | 3.7% | 7.3% | 34 | 7425 |
| mass sample w/ $\geq$1 $b$ SVX tag | 3.0% | 5.8% | 20 | 6000 |
| mass sample w/ $\geq$2 $b$ SVX tags | 0.52% | 1.8% | 5 | 1800 |

Table 2.2:
Acceptance and yield of $t\bar{t}$ events for a Run IIb upgraded detector. The yield is determined using the theoretical cross section (6.8 pb) at $m_{top} = 175$ GeV/c$^2$, $\sqrt{s} = 2$ TeV, and 15 fb$^{-1}$ data sample. For comparison, the acceptances for Run Ib are shown as well as the number of events seen in Run 1 prior to background subtraction. The acceptances include branching ratios and leptonic and kinematic selection (*e.g.* jet counting).

CMX detector (at higher $|\eta|$) were used to identify secondary leptons only — the very high rates and dynamic prescales used in the trigger proved too difficult to untangle. Much of this problem has been addressed for Run IIA by substantially increasing the steel shielding between the interaction region and these counters. This shielding should reduce the number of fake hits such that the trigger rates in the CMX region will be manageable.

Since the drift times in the muon chambers are now appreciably longer than the bunch crossing, scintillation counters, which shadow all of the muon chambers, were added so that muon stubs can be assigned to a particular bunch crossing. Some of this scintillator, like those mounted on the CMX muon arch chambers were installed in Run I and are now showing signs of aging. Current aging projections show that the performance of these counters will be substantially degraded in the next 2-3 years. If it is not replaced, this region of rapidity unusable for top physics in Run IIb. This loss would decrease the muon acceptance by approximately 10% from Run IIA.

- **Central Calorimeter**: With the increased luminosity and smaller bunch spacing of Run IIB, the central preshower and central crack chambers will need replacement. Their relatively poor segmentation and slow readout times will render these detectors useless in this new environment. The loss of these detectors will cripple both electron and photon identification - both critical to top quark physics. The central preradiator in Run I offered a factor of 2 to 3 more rejection of charged pions that pass all other cuts using tracking, calorimetry, and shower maximum information. This extra rejection is crucial in minimizing background in soft electron ID for b-jet tagging (SLT).

### 2.3.4 Event Yield

To estimate the yield of top events, we extrapolate from our current measured acceptance in Run I using the theoretical cross section (6.8 *pb*) at $m_{top} = 175$ GeV/c$^2$ and $\sqrt{s} = 2$ TeV [22, 11].

At $\sqrt{s}$ =2 TeV, the $t\bar{t}$ cross section is approximately 40% higher than at $\sqrt{s}$=1.8 TeV. We assume that the additional lepton and $b$-tagging acceptance outlined in Sec. 2.3.3 above can be incorporated while maintaining a signal-to-background ratio comparable to the Run I analysis.

Table 2.2 summarizes the acceptance and yields for various decay channels in the Run II configuration. The Run Ib acceptances are shown for comparison. A data sample of 15 fb$^{-1}$ at the Tevatron will provide over 7500 identified $b$-tagged $t\bar{t}$ events.

### 2.3.5 Measurement of the Top Quark Mass

The top quark mass will be one of the most important electroweak measurements made at the Tevatron. In combination with the W mass, $m_t$ gives information about the mass of the standard model Higgs boson. The precision electroweak program and the W mass measurement are discussed in the electroweak section of Chapter 2. Figure 2.14 shows how the predicted top and W mass measurements constrain the Higgs mass. In that figure, the uncertainty on the top mass is taken as 4 GeV/c$^2$.

Currently, the statistical and systematic uncertainties on CDF's top mass measurement are both about 5 GeV. The statistical uncertainty should scale as $1/\sqrt{N}$. Using the yields in Table 2.2, we anticipate that the statistical uncertainty on the top mass in the optimized lepton+$\geq$ 4-jet sample will be much less than 1 GeV/c$^2$. Thus in Run IIb, the overall uncertainty will be dominated by systematics. In fact, we expect approximately 1800 double-tagged lepton+$\geq$ 4-jet events on tape with a 15 fb$^{-1}$data sample. That one sample alone is sufficiently large that the statistical uncertainty will be less than 1 GeV. Since both b-jets are identified in the double-tagged subsample, it may turn out that the systematics for these events are better understood. If this is the case, there would be no need to include the other 3 subsamples (no-tag, single SVX tag, SLT tag) as was done in Run I.

Almost all of the systematic uncertainties in the top mass measurement are coupled to the reliability of the Monte Carlo models for the spectrum of fit masses in signal and background. Assuming the theory model is accurate, most of the uncertainty is related to resolution effects. Instrumental contributions include calorimeter nonlinearity, losses in cracks, dead zones, and absolute energy scale. A larger and more difficult part of the energy resolution concerns the reliability of the extrapolation to parton energies. Ultimately, it may be our understanding of QCD and not the detector which limits the mass resolution.

Many of these issues can be addressed by *in situ* calibration procedures. For example, Z+jet events are used to understand the systematic uncertainty due to energy scale and gluon radiation, two of the dominant uncertainties. In 15 fb$^{-1}$, we expect to have 200K (525) Z's with 1 (4) or more jets. The effect of gluon radiation will also be studied in large statistics samples of W+jets, $\gamma$+jets, and $b\bar{b}$ events. In addition, the mass peak from $W \to qq'$ (see Figure 2.17) in the lepton + jets top sample allows an energy scale calibration *in exactly the same events and environment* as the mass measurement. [1].

In any case, if all systematic effects can be measured or otherwise connected with mean quantities in large statistics control samples, the systematic uncertainties should also scale as $1/\sqrt{\mathcal{L}}$. We can conservatively assume in this case that we can reduce our systematic error to $\approx 2$ GeV/c$^2$.

### 2.3.6 Production Cross Section, $\sigma_{t\bar{t}}$

An accurate measurement of the $t\bar{t}$ production cross section is a precision test of QCD. A cross section which is significantly higher than the theoretical expectation would be a sign of non-standard model production mechanisms, for example the decay of a heavy resonant state into $t\bar{t}$ pairs or anomalous couplings in QCD. As in the case of the top mass, large statistics in the lepton+jets mode imply that systematic uncertainties will be the limiting factor in the cross section measurement.

For the acceptance, the reliability of jet counting and $b$-tagging are at issue. Initial state radiation can be examined using a sample of Z+jets, while the jet energy threshold uncertainty can be addressed as in the top mass discussion. With 15 fb$^{-1}$ of data it will be possible to measure the $b$-tagging efficiency *in top events*, using dilepton events selected without a $b$-tag and the ratio of single to double tags in lepton+jets events. We assume that these studies will give uncertainties that scale as $\sqrt{N}$. Hence we expect of order a 3 fold improvement in these systematic uncertainties from what was estimated for Run IIa.

With large samples, one can measure the bottom and charm content as a function of jet multiplicity in W + jet events using the c$\tau$ distribution of the tagged jets and use this to tune the Monte Carlo models for W+$\geq$ 3-jet backgrounds. Finally, in Run II and beyond, the luminosity will be measured either through the $W \to l\nu$ rate, or the mean number of interactions per crossing, and we will assume 5% for the future precision of the luminosity normalization.

Accounting for all effects we find that the total $t\bar{t}$ cross section can be measured with a precision of $\approx$ 5% for 15 fb$^{-1}$. This will challenge QCD, and provide a sensitive test for non-standard production and decay mechanisms.

### 2.3.7 Measurement of a t → W Branching Fraction

The ratio of the $t\bar{t}$ cross section measured using dilepton events to that measured using lepton+jets events is a test for non-standard model decay modes of the top quark. Since the cross section in each case assumes that each top decays into W-bosons, a ratio different from 1.0 would signal decays *without* a W-boson, such as charged Higgs (t → $H^+$ b) or light supersymmetric top (stop). The reach for a particular non-standard decay is model dependent, but we can say that with 15 $fb^{-1}$ of data, we will be able to measure the basic dilepton to lepton+jets ratio to 8%, and the top branching fraction to W in association with $b$ with a precision of 5%.

### 2.3.8 Measurement of a t → b Branching Fraction

In the standard model with 3 generations, existing experimental constraints and the unitarity of the CKM matrix require $V_{tb} \simeq 1$, predicting that the weak decay of the top will proceed almost exclusively through W + b. In events containing a W, the top branching fraction to b's is related to the CKM element according to:

$$\begin{aligned} B_b &= B(t \to W(b)) \\ &= \frac{\sigma(t \to Wb)}{\sigma(t \to Wq)} \\ &= \frac{|V_{tb}|^2}{|V_{td}|^2 + |V_{ts}|^2 + |V_{tb}|^2} \end{aligned}$$

The notation above is meant to indicate that a W has been required in the final state, and this is not the decay fraction to W+b, but the fraction of decays with W's which *also* contain b's. Since the standard analysis identifies $t\bar{t}$ events by requiring at least 1 W and 1 b, $B(t \to W(b))$ is measured from the number and distribution of tagged $b$-jets in top events. Four different techniques can be used to measure this distribution: [20, 21]

- The ratio of double $b$-tagged to single $b$-tagged events in the $b$-tagged lepton+jets sample: requiring one $b$-jet to be tagged leaves the second jet unbiased, and from a known tagging efficiency, one can extract the branching ratio from the ratio of tagged to untagged "second jets". [20]
- The ratio of single $b$-tagged to no $b$-tagged events in a lepton+jets sample in which kinematic criteria have been applied: since there is no a-priori tag requirement, we can extract the branching ratio from the ratio of single tagged events to not-tagged events. An ideal sample for this is the W+4 jet mass sample prior to applying the $\chi^2$ cut. [21]
- The number of $b$-tagged jets in the dilepton sample: Since $b$-tagging is not required to identify tops decaying to dileptons, the whole $b$-tag multiplicity distribution in these events contains information on $B(t \to W(b))$. Despite the smaller branching fraction to dileptons, the statistical powers of the dilepton and lepton+jets samples are comparable.
- The distribution of double tags: If there are two tagging algorithms (soft leptons and secondary vertex), one can compare the number of times that events tagged by both algorithms have both tags in the same jet vs. the number of times the tags are in different jets. Small values of $B(t \to Wb)/B(t \to Wq)$ result in large values of the same to different jet ratio.

These techniques are not exclusive, and can be combined. We have used a maximum likelihood estimator to do this combination in Run I data. With 105 $pb^{-1}$, CDF has a ±25% statistical uncertainty on the branching fraction, but only an ±11% systematic uncertainty. The systematic uncertainty is dominated by the uncertainty on the tagging efficiency, which is measured in the data using $b$-rich inclusive lepton samples. This uncertainty should fall as $1/\sqrt{N}$. The small non-$t\bar{t}$ backgrounds will be measured to high accuracy by Run II. For Run II, we expect to measure $B(t \to W(b))$ to 3.0%.

### 2.3.9 Anomalous Couplings and Weak Universality

Since the top quark is so heavy, it is possible that the physics of the underlying theory may manifest itself via new non-universal top interactions. The top quark is unique in that it decays prior to hadronization and therefore the decay products carry helicity information related to the fundamental couplings. In the standard model, the top quark decays only to longitudinal or left-handed W's, where the ratio is given by

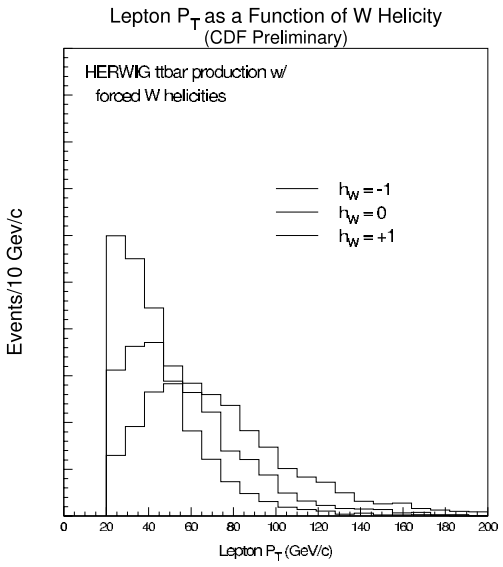


Figure 2.18: The lepton Pt as a function of W helicity for 175 GeV $t\bar{t}$ events

$$\frac{W_{long}}{W_{left}} = \frac{1}{2}\left(\frac{m_{top}}{m_W}\right)^2$$

For $m_{top} = 175.9$ GeV/$c^2$, the branching fraction to longitudinal W's is $70.6 \pm 1.6\%$. In many cases non-universal top couplings will appear as as a departure of $\mathrm{B}(t \to bW_{\mathrm{long}})$ from the standard value and we use this quantity as our precision benchmark for probes of anomalous weak couplings.

Experimentally, we have two ways to access the polarization state of the decay W. The first way and perhaps the most obvious way is through the charged lepton helicity angle, $cos\theta_e^*$ which can be measured in the lab frame as

$$\cos\theta_e^* \approx \frac{2M_{eb}^2}{m_{eb\nu}^2 - M_W^2} - 1 \qquad (2.1)$$

The resulting distribution can then be fit to a superposition of W helicity amplitudes in order to measure any possible contribution of non-universal weak couplings in the top decay.

The second way uses the shape of the lepton Pt spectra. The idea here is that the charged lepton from the left handed W tends to move opposite to the W direction while that from the longitudinal W tends to be perpendicular to the W direction. In the lab frame, this implies that leptons from longitudinal W's have a somewhat harder Pt distribution than those from the left-handed W's. See Figure 2.18 for an illustration using Herwig MC.

For Run 1 data, it turned out that both techniques have roughly equal statistical sensitivity, but $P_T$ offers many advantages over the angular distribution. It eliminates systematic uncertainties related to parton combinatorics and neutrino reconstruction in the mass fitter and as a variable is more accurately measured.

The following cuts were used in the Run 1 analysis [40, 41]. We start with the cuts used in the $t\bar{t}$ cross-section analysis for event selection and then pick 4 subsets out of this W+3 jet heavy flavor data set.

- A displaced vertex tag identified by our algorithm SECVTX.
- A 4th lower energy jet ($E_T > 8$ GeV) and a soft lepton tag (SLT) within a cone of 0.4 of one of the 3 leading jets and NOT have a SECVTX tag
- A 4th high energy jet ($E_T > 15$ GeV) and a mass fitter value $\chi^2 < 10$.
- Standard dilepton search criteria

A likelihood procedure is performed using the lepton Pt as a variable to determine the fraction of top quarks which decay to longitudinal W bosons. For 105 pb-1, the fraction of top quarks which decay longitudinally is 0.91 ± 0.37 (stat) ± 0.13 (syst). The fraction of top quarks which decay to right handed W bosons (helicity of +1) is measured to be 0.11 ± 0.15 (stat) ± 0.06 (syst). The dominant systematic contributions are due to the uncertainty in top mass and the relative fractions of background contributions.

To date, no study has been performed to see how one would measure this quantity in Run IIb. The data samples will be significantly larger which would help measure the polarization angle. However even with double tagged events, there is still a bias due to mass fitter. It is important to note that even with relatively small data samples in run 1, the systematic uncertainty on this measurement is already quite small. With 15 fb$^{-1}$of data, we should be able to measure the top quark decay branching fraction to longitudinal W-bosons with a total precision approaching of order 1%. The V+A term in top decay should have similar sensitivity.

### 2.3.10 Single Top Quark Production

In addition to $t\bar{t}$ pair production via the strong interactions, top quarks can also be produced singly via the electroweak interaction. This process depends on the t-W-b vertex, and the production rate is a measure of the top decay width to W+b and the CKM matrix element $|V_{tb}|^2$. Single top is of theoretical interest because it provides a direct window on the charged-current interaction of the top quark. Unlike the case of top pair production where the electroweak vertex tWb plays a role only in the top quark's decay, in single top, the production cross section contains information on the coupling of top to W and $b$. Thus the production cross-section for single top contains information on the top partial width.

So far, we have assumed the validity of the Standard Model. Nonstandard couplings could invalidate the above simple extrapolation between $V_{tb}$ and the top width or even render the entire concept of $V_{tb}$ ill defined. Examples of proposed anomalous couplings that could impact single-top production rates include a $q^2$-dependent form factor at the $tWb$ vertex or new flavor-changing neutral current couplings like $tZc$ or $tgc$. New particles such as heavy $W'$ boson would also lead to unexpected rates of single top production. Thus measuring single-top production is a win-win proposition. Either we get information on the top width and $V_{tb}$ or we find evidence of new physics.

The two dominant single top processes at the Tevatron are the s-channel mechanism $qq \to t\bar{b}$, referred to here as $W^*$ production, and the t-channel interaction $qb \to qt$, referred to as W-gluon fusion. Other processes become important at higher energies, but are negligible here because they have such heavy final states. Based on theoretical calculations, the W-gluon fusion process is thought to dominate the production with an estimated cross section of 1.7 pb at a 900 GeV Tevatron; the uncertainties on this calculation are on the order of 15%. The $W^*$ production mode is roughly half as large and has an estimated cross section of 0.73 pb with a theoretical uncertainty of 9%. The combined rate for single top production by these two processes is $\approx$ 2.4 pb, only a little more than a factor of 2 down from the $t\bar{t}$ rate at this energy.

As is the case for $t\bar{t}$, single top events present themselves in the CDF detector as the leptonic or hadronic W decay products accompanied by one or more additional jets. Single top events are interspersed among a vast background of QCD processes which appear as energetic jets in the detector. Since hadronic W decay products are not easily distinguished from ordinary QCD jets, a first step in isolating the single top signal is to demand evidence of a leptonic W-decay as is done with $t\bar{t}$ - namely applying leptonic W selection criteria of a high Pt electron or muon plus large missing energy. As in $t\bar{t}$, dilepton and Z removal cuts are used to reduce unwanted backgrounds further. B-tagging is also used. What remains are backgrounds of W+heavy flavor and $t\bar{t}$ production. Thus, additional cuts are required to separate single top events from these backgrounds.

There are differences between the final states in Wg fusion and $W^*$ production. The final state for $W^*$ production features a second high-$P_t$ central b-jet in addition to the $b$ coming from the top decay $t \to Wb$. The second $b$ in a W-gluon event is expected to be soft and forward and thus not detectable as such in the CDF detector. Furthermore, the $Wg$ event is expected to contain an additional hard forward light-quark jet. Cuts must be developed with these differences in mind to isolate the individual processes.

The data selection criteria that were used to isolate the signal over background in the Run I analysis include:

- High $P_T$ lepton events with 1, 2, or 3 jets with $E_T > 20$ GeV, $|\eta|_{\text{jets}} < 2.4$
- $\not\!\!E_T > 20$ GeV
- $E_T(\text{electron}) > 20$ GeV
- $|\eta|_{\text{electron}} < 1.0$
- Z and Dilepton removal
- At least one jet tagged as a $b$-jet.
- Reconstruct mass of lepton, neutrino and b-tagged jet to be inside the window $140 < M_{l\nu b} < 210 GeV$
- Fit the $H_T$ distribution where $H_T$ is the energy of the jets, leptons and MET in the event

After selection cuts we expect a 4.3 signal events (W* and Wgluon combined) and 62 background events. Thus we expect a $S/\sqrt{B} = 0.5$. See Table 2.3 for a breakdown by bin and by data sample type. A likelihood fit is then performed based on the variable $H_T$ and a 95

| Process | $W+1J$ | $W+2J$ | $W+3J$ |
|---|---|---|---|
| $Wg$ Signal | 0.80 | 1.50 | 0.71 |
| $W^*$ Signal | 0.25 | 0.80 | 0.23 |
| $t\bar{t}$ Bckg | 0.21 | 2.28 | 5.91 |
| QCD Bckg | 37.4 | 13.9 | 2.7 |
| Total | 38.7 | 18.5 | 9.6 |

Table 2.3:
Bin by Bin predictions for the single top processes and backgrounds for a data size of 105 pb.

The above analysis was optimized for a small statistical data set. With the large samples expected in Run IIb, one could remove the 1 jet bin, cut harder on some of the kinematic variables and separate out the two separate single top processes. By just removing the 1 jet bin for large data samples, the S/$\sqrt{B}$=2.9! Based on the theoretical cross section and acceptances from this analysis, one could expect to see roughly 100 $W^*$ events in the W+2 jet bin per fb$^{-1}$ and 150 $Wg$ events per fb$^{-1}$. Hence in Run IIb, we expect a total sample of single top events to be of order 4000 events on tape. Assuming that the background normalization is understood (through the large statistics top cross section measurement), the statistical precision on the single top cross section using 15 fb$^{-1}$ will be about $\tilde{1}0\%$.

Many of the sources of systematic uncertainty in the single top cross section are common to the $t\bar{t}$ cross section discussed earlier. We assume that systematic uncertainties related to selection efficiencies and backgrounds will shrink as $\sqrt{N}$. For the case of 15 fb$^{-1}$ we find that the measurement of the single top cross section will have a total uncertainty of approximately 12%.

The single top cross section is directly proportional to the partial width $\Gamma(t \to Wb)$ and assuming there are no anomalous couplings, this is a direct measure of $|V_{tb}|^2$. There are theoretical uncertainties in converting the cross section to the width, notably for the gluon fusion process. Taking these into account, we anticipate that a measurement of the total single top rate with 15 fb$^{-1}$ will translate in a precision of 6% on $|V_{tb}|$.

The theoretical determination of W* is more reliable than that of W-gluon fusion since initial state effects can be measured in the similar Drell-Yan process, and if the data set is large enough this may afford the best precision on the width. The two processes can be separated by requiring two b-tags since the double tag rate for W* production is close to a factor of 5 more than that of W-gluon fusion.

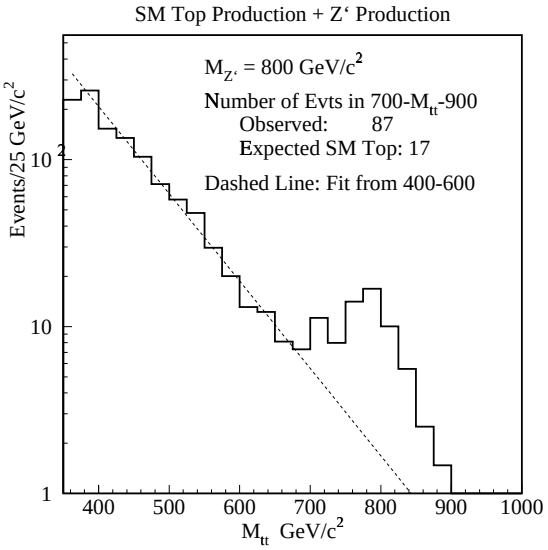


Figure 2.19: A hypothetical $m_{t\bar{t}}$ spectrum with an 800 GeV/c$^2$ Z′ topcolor boson. The rate is based on the theoretical predicted cross section for $t\bar{t}$ production and Z′ production [31] with 2 fb$^{-1}$.

### 2.3.11 Search for Anomalously Large Rare Decays

- $t \to Zc, \gamma c$
- $t \to WZb$
- $t \to W^+W^-c$
- $t \to Hc$

The standard model predicts that the branching fractions of FCNC top decays are around $10^{-10}$ [29],

out of reach for even the LHC. Any observation of such decays will signal new physics. As illustration, we consider the signal for a flavor changing neutral current decay $t \to c\gamma$ in a $t\bar{t}$ event. If the other top in the event decays in the leptonic channel, the acceptance is almost the same as the standard model lepton+jets mode, and it then becomes a simple matter to scale from present results. The background from $W + \gamma +$ two jets is about 1 fb. Although it is unlikely that this background will be kinematically consistent with $t\bar{t}$ (for example, that $m(\gamma+j) = m(t)$), we take the very conservative assumption that this background is irreducible. We find that 15 fb$^{-1}$ will probe branching fractions for this decay down to $1.0 \times 10^{-3}$

Sensitivity to other rare decays can be scaled from this estimate. For the case $t \to Z + c$, where the $Z$ decays to leptons, after adjusting for branching ratios and different backgrounds, we find sensitivity down to of order 0.5%.

#### 2.3.11.1 Dynamical Symmetry Breaking

Because of its large mass, the top quark is an excellent probe for physics beyond the standard model. Theories which implicate top in the electroweak symmetry breaking mechanism, such as a color-octet vector meson associated with a top condensate[33] or multiscale technicolor[34], predict enhancements or changes in the shape of the $t\bar{t}$ invariant mass spectrum ($m_{t\bar{t}}$) and the top quark transverse momentum distribution ($P_T^{top}$).

CDF performed a search for resonances, $X \to t\bar{t}$, in the $M_{t\bar{t}}$ spectrum by reconstructing $M_{t\bar{t}}$ on an event-by-event basis using the same event sample and constrained fitting techniques used in the top mass measurement, with an additional constraint that the top mass. Effectively once the fit for $M_{t\bar{t}}$ is done, one then looks at the 3 body masses and asks whether they "wanted" to be fit to top. 63 events satisfied the selection criteria. The $M_{t\bar{t}}$ distribution of 63 data events yields a $\chi^2$ of 80% when compared to the hypothesis that the spectrum is comprised of Standard Model $t\bar{t}$ production and the predicted rate of non-$t\bar{t}$ background events. A 95% confidence level cross-section limits for generic objects in the mass range of 400 GeV/$c^2$ to 1 TeV/$c^2$ which decay to $t\bar{t}$. These results exclude the existence of a lepto-phobic top-color Z‘ with masses less than 480 GeV/$c^2$ for $\Gamma = 0.012$M and 780 GeV/$c^2$ for $\Gamma = 0.04$M.

In the absence of a signal, limits in Run II will be as high as 1000 GeV/c$^2$. New resonances with masses below the limit could be observed. For example, Figure 2.19 shows the $M_{t\bar{t}}$ spectrum for 2 fb$^{-1}$ with standard model $t\bar{t}$ production plus the addition of a top-color Z$'$ at 800 GeV/c$^2$ [31], where the Z$'$ decays to a $t\bar{t}$ pair. In this theory, the branching fraction of Z$'$ to $t\bar{t}$ pairs is potentially large (50-80%) but depends on the Z$'$ width. In the case shown in Figure 2.19, we would expect 17 events from standard model $t\bar{t}$ production in the range $700 < M_{t\bar{t}} < 900$ GeV/c$^2$ and 70 events from Z$' \to t\bar{t}$ in this range. The $M_{t\bar{t}}$ spectrum along with other $t\bar{t}$ production distributions provide an excellent means for searching for new phenomena.

### 2.3.12 Summary of Top Physics

For the next 5 years, the Tevatron will be the only accelerator capable of producing the top quark. Maintaining the capability of the CDF Run IIa detector is critical for setting limits on rare top searches, understanding the production rates for single top, and first significant measurements of both the top width and $V_{tb}$ as well as on advancing the precision of Run IIa measurements.

The top physics program possible with this sample is summarized in Table 2.4. Measurements of branching ratios, angular distributions, and top production mechanisms with the sensitivities listed in Table 2.4 will provide the first complete characterization of this new fermion and provide another stringent test of the Standard Model. Our catalog of possible measurements is hardly complete. But in the event that the top quark yields surprises, these sensitivities benchmark the capability to explore new physics at the Fermilab Tevatron.

| Measurement | 15 fb$^{-1}$ | Comment |
|---|---|---|
| Yields | | |
| $N_{3jet*b}$ | 7500 | *identified* events |
| $N_{4jet*2b}$ | 1800 | clean $m_t$ sample |
| $\delta m_t$ | 2 | total precision GeV/$c^2$ |
| Production | | |
| $\delta\sigma_{t\bar{t}}$ | 6% | test top QCD couplings |
| $\delta\sigma_{ll}/\sigma_{l+j}$ | 9% | test non W decay |
| $\delta\sigma_{t\bar{b}X+b\bar{t}X}$ | 12% | isolate "single top" |
| Decay | | |
| $\delta B(t \to W(b))$ | 1% | from N(bb)/N(bX) |
| $\delta B(t \to b(W))$ | 3% | from N(ll)/N(lX) |
| $\delta B(W_{V+A})$ | 1% | $W \to l\,\nu$ helicity |
| $\delta B(W_{long})$ | 1% | $\frac{W_{long}}{W_{left}} = \frac{1}{2}(\frac{m_{top}}{m_W})^2$ |
| $\delta V_{tb}$ | 6% | from above |
| Rare Decays | | |
| B(c $\gamma$) | $\leq 1 \times 10^{-3}$ | (95% CL) |
| B(cZ) | $\leq 5 \times 10^{-3}$ | (95% CL) |
| B(Hb) | $\leq 9\%$ | from $\sigma_{ll}/\sigma_{l+j}$ |

Table 2.4: Summary of expected measurement accuracies for an integrated luminosity of 15 fb$^{-1}$

# Bibliography


[1] *Future ElectroWeak Physics at the Fermilab Tevatron: Report of the TeV_2000 Study Group*, Editors D. Amidei and R. Brock Fermilab–Pub–96/082

[2] F. Abe *et al.* (CDF Collaboration), Phys. Rev. D **50**, 2966 (1994); F. Abe *et. al.* (CDF Collaboration), Phys. Rev. Lett. **73**, 225 (1994).

[3] F. Abe *et al.* (CDF Collaboration), Phys. Rev. Lett. **74**, 2626 (1995).

[4] S. Abachi *et al.* (D0 Collaboration), Phys. Rev. Lett. **74**, 2632 (1995).

[5] F. Abe *et al.* (CDF Collaboration), Phys. Rev. D **52**, R2605 (1995).

[6] F. Abe *et al.* (CDF collaboration), Phys. Rev. Lett. **75**, 3997 (1995).

[7] M. Hohlmann, *Observation of Top quarks in the dilepton decay channel* $t\bar{t} \rightarrow e(\mu)\nu_{e(\mu)}\ \tau\nu_\tau\ b\bar{b}$ *Using Hadronic Tau Decays At CDF*, Proc., Lake Louise Winter Institute (1996)

[8] P. Azzi *et al.*, *Hadronic Top Production at CDF*, CDF Note 3679.

[9] R. Hughes, B. Winer, T. Liss, *Combining the SVX, SLT, and Dilepton* $t\bar{t}$ *Cross Sections*, CDF Note 3111.

[10] T. Liss, R. Roser, $t\bar{t}$ *Production Cross Section for 110* $pb^{-1}$, CDF Note 3481.

[11] A. Beretvas, Int. J. Mod. Phys. A11, 2045 (1996)

[12] P. Azzi *et al.*, $t\bar{t}$ *Production Cross Section in the All-hadronic Channel*, CDF Note 3464.

[13] K. Tollefson *et al.*, *Optimizing the Top Quark Mass Measurement*, CDF Note 3606.

[14] S. Aota *et al.*, *Update to Top Mass on Double b-tagged Events Using Loose Jet Probability Tagging*, CDF Note 3604.

[15] R. Wilkinson *et al.*, *Update to Hadronic W Decays in Double b tagged Top Candidates*, CDF Note 3543.

[16] E. Malkawi, C.-P. Yuan, *A Global Analysis of the Top Quark Couplings to Gauge Bosons*, Phys. Rev. D **50**, R4462 (1994).

[17] E. Laenen, J. Smith, W.L. van Neerven, Phys. Lett. **321B**, 254 (1994).

[18] Catani, Mangano, Nason and Trentadue, CERN Preprint, CERN-TH/96-21 hep-ph/9602208.

[19] E. Berger, Argonne Nat. Lab. Preprint ANL-HEP-PR-95-31

[20] T. LeCompte, R. Roser, *Measurement of* $BF(t \rightarrow Wb)$ *and the CKM Matrix Element* $|V_{tb}|$ *in Top Decays*, CDF Note 3056.

[21] F. Bedeschi, G. Chiarelli, F. Tartarelli, *Measurement of* $BF(t \rightarrow Wb)$ *in Top Decays*, CDF Note 3853.

[22] E. Laenen, private communication.

[23] R. Hughes, R. Roser, from a series of talks at the CDF upgrade meetings

[24] D. Atwood, A. Kagan, T.G. Rizzo, *Constraining Anomalous Top Quark Couplings at the Tevatron*, SLAC-PUB-6580, July 1994.

[25] G. Kane, C.-P. Yuan, and D. Ladinsky, Phys. Rev. D **45**, 124, (1992); D. Atwood, A. Aeppli, and A. Soni, Phys. Rev. Lett. **69**, 2754, (1992); R.S. Chivukula, S.B. Selipsky, E.H. Simmons, Phys. Rev. Lett. **69**, 575, (1992); M.Peskin, talk presented at the *Second International Workshop on Physics and Experiments at a Linear e+e- Collider*, Waikoloa, HI, April 1993; M.Peskin and P. Zerwas, talks presented at the *First International Workshop on Physics and Experiments at a Linear e+e- Collider*, Saariselka, Finland, September 1991.

[26] S. Dawson, Nucl. Phys. **B249**, 42 (1985); S.S.D. Willenbrock and D.A. Dicus, Phys. Rev. D **34**, 155 (1986); S. Dawson and S.S.D. Willenbrock, Nucl. Phys. **B284**, 449 (1987); C.-P. Yuan, Phys. Rev. D **41**, 42 (1990); S. Cortese and R. Petronzio, Phys. Lett. **B253**, 494 (1991); G.V. Jikia and S.R. Slabospitsky, Phys. Lett **B295**, 136 (1992), R.K. Ellis and S. Parke, Phys. Rev. D **46**, 3785 (1992); G. Bordes and B. van Eijk, Z. Phys. **C57**, 81 (1993); G. Bordes and B. van Eijk, Nucl. Phys. **B435**, 23 (1995): T. Stelzer and S. Willenbrock, Phys. Lett. **B357**, 125-130 (1995).

[27] D. Winn, D. Amidei, *Study of the $t \to Wb$ Vertex at CDF*, CDF Note 2914.

[28] D.O.Carlson, C.-P. Yuan, Phys. Lett. **306B**, 386 (1993).

[29] S. Parke, *Summary of Top Quark Physics*, FERMILAB -Conf-94/322-T. Presented at DPF'94, University of New Mexico, Albuquerque, NM, August 2-6, 1994.

[30] T. Stelzer, S. Willenbrock, *Single-Top-Quark Production via $q\bar{q} \to t\bar{b}$*, DTP/95/40, ILL-(TH)-95-30 (1995).

[31] C. Hill, *Topcolor Assisted Technicolor*, Fermilab-Pub-94/395-T

[32] K. Lane, *Top Quarks and Flavor Physics*, BUHEP–95–2.

[33] C. T. Hill, Physics Lett. **266B**, 419 (1991).

[34] K. Lane, E. Eichten, Phys. Lett. **222B**, 274 (1989); K. Lane and M.V. Ramana, Phys. Rev. D **44**, 2678, (1991).

[35] CDF Collaboration, *Technical Design Report for Run II*, Fermilab-pub-96/390-E.

[36] G. Apollinari et al, *Method II measurement of the top cross section with W+3,4 jet events with SECVTX, JPB and SLT tags*, CDF Note 4303.

[37] The Top Group, *The New CDF Run 1 combined $t\bar{t}$ production cross section*, CDF Note 5043.

[38] J. Cassada, P. Tipton, M. Kruse, *Consistency of the Run 1 Top Dilepton Candidate Events with the Top Quark Hypothesis* , CDF Note 4268.

[39] P. Azzi, W. Bokhari, A. Castro, *The effect of the new scale factor on the combined $t\bar{t}$ cross-section in the All Hadronic Channel*, CDF Note 5044.

[40] D. Winn and D. Amidei, *Measurement of W Helicity Fractions in Top Decay*, CDF Note 4464.

[41] D. Winn and D. Amidei, *Update to the Measurement of W Helicity Fractions in Top Decay* , CDF Note 4673.

[42] S. Wolinski P. Savard, *An upper limit on Standard Model single top production in CDF Run 1 data using fitting techniques* , CDF Note 5199.

[43] S. Truitt, P. Savard, *Search for Single Top Production in CDF Run 1 Data* , CDF Note 4978.

[44] First Measurement of Br(t-¿Wb)/Br(t-¿Wq) and Associated Limit on the Cabbibo-Kobayashi-Masakawa Element —Vtb— F. Abe *et al.* (CDF Collaboration), Phys. Rev. Lett. **86**, 3963 (2001).

[45] Measurement of the t-tbar Production Cross Section F. Abe *et al.* (CDF Collaboration), Phys. Rev. **D64**, 032002 (2001).

[46] Measurement of the Top Quark Mass at CDF F. Abe *et al.* (CDF Collaboration), Phys. Rev. **D63**, 032001 (2001).

[47] Measurement of the Helicity of W Boson in Top Quark Decays F. Abe *et al.* (CDF Collaboration), Phys. Rev. Lett. **84**, 216 (2000).

[48] Search for New Particles Decaying to t-tbar in p-pbar Collisions at $\sqrt{s}$ =1.8 TeV F. Abe *et al.* (CDF Collaboration), Phys. Rev. Lett. **85**, 2062 (2000).

[49] Measurement of the Top Quark Mass with the Collider Detector at Fermilab F. Abe *et al.* (CDF Collaboration), Phys. Rev. Lett. **82**, 271 (1999).

[50] Erratum: Measurement of the Top Quark Mass with the Collider Detector at Fermilab F. Abe *et al.* (CDF Collaboration), Phys. Rev. Lett. **82**, 2808 (1999).

[51] Observation of Hadronic W Decays in t-tbar Events with the Collider Detector at Fermilab F. Abe *et al.* (CDF Collaboration), Phys. Rev. Lett. **80**, 5720 (1998).

[52] Measurement of the Top Quark Mass and Production Cross Section from Dilepton Events at CDF F. Abe *et al.* (CDF Collaboration), Phys. Rev. Lett. **80**, 2779 (1998).

[53] Measurement of the t-tbar Production Cross Section in p-pbar Collisions at $\sqrt{s} = 1.8$ TeV F. Abe *et al.* (CDF Collaboration), Phys. Rev. Lett. **80**, 2773 (1998).

[54] Measurement of the Top Quark Mass F. Abe *et al.* (CDF Collaboration), Phys. Rev. Lett. **80**, 2767 (1998).

[55] Search for FCNC of the Top Quark Decay F. Abe *et al.* (CDF Collaboration), Phys. Rev. Lett. **82**, 2525 (1998).

[56] Search for New Particles Decaying into b-bbar and Produced in Association with W Bosons Decaying into e-nu or mu-nu at the Fermilab Tevatron F. Abe *et al.* (CDF Collaboration), Phys. Rev. Lett. **79**, 3819 (1997).

[57] First Observation of the All-Hadronic Decay of t-tbar pairs F. Abe *et al.* (CDF Collaboration), Phys. Rev. Lett. **79**, 1992 (1997).

## 2.4 Precision Electroweak Program

### 2.4.1 Introduction

The comparison of diverse precision experimental measurements to expectations from the Standard Model [1] allows precise tests sensitive to new physics at scales above the electroweak scale, as well as a determination of the Higgs mass within the framework of the model [2]. Global electroweak fits receive contributions from LEP, LEPII and SLC, $W$ mass measurements in $\bar{p}p$ interactions, neutrino neutral current data, and the measurement of the top mass at the Tevatron.

Precision measurement of the top mass and the $W$ mass are primary goals of CDF II. In addition, in the electroweak sector, the $W$ width and leptonic branching ratio, the tri-linear couplings of the $W$, $Z$ and $\gamma$, and the forward-backward charge asymmetry of dileptons at the $Z$ pole and above are important Standard Model parameters. These measurements together will take the global electroweak fit to a new level of precision, and do so completely in the context of a single experiment.

In this section we discuss measurements directly involving the gauge bosons. We begin with a comparison of the the expected event yields of $W$, $Z$, and diboson production for Run IIa with 2 fb$^{-1}$ and Run IIb with 15 fb$^{-1}$, which illustrates the electroweak physics potential (see Table 2.5). We then discuss the CDF Electroweak measurement prospects for Run IIb.

Studies of the Run II sensitivities for Electroweak physics at CDF II, and their competitiveness with LEP-II, LHC and NLC experiments are detailed in the Summary Report of the Workshop on QCD and Weak Boson Physics in Run II [3]. A review of the Run I results on $W$ boson physics can be found in [4].

### 2.4.2 Impact of Proposed Run IIb Upgrades

Most of the proposed Run IIb upgrades are aimed at maintaining the enhanced detector capabilities that were achieved over Run I by the Run IIa upgrades. Apart from the obvious need to maintain triggering and data acquisition capability in order to record the large data samples, we mention the relevant detector upgrades for electroweak physics.

The momentum measurement from the COT is clearly very important for leptons. At very high instantaneous luminosities, the occupancy in the inner superlayers will hurt pattern recognition and track resolution. The proposed upgrades to the COT inner layers and the silicon detector are both relevant for maintaining track efficiency and quality.

#### 2.4.2.1 Electrons

The detection capabilities for forward electrons and photons were significantly enhanced over Run I by the plug calorimeter and the SVX II+ISL+COT integrated tracking. The charged tracking and momentum information will be better, more efficient, and available over a wider range in $\eta$. Plug electrons will significantly improve the yields for W and Z bosons, and allow us to examine some previously inaccessible electroweak physics topics at high $\eta$. When considering the purely leptonic decay modes, the acceptance for $W$ bosons is almost doubled, for $Z$ bosons tripled, and for the rarer diboson modes quadrupled by increasing the electron coverage from $|\eta| < 1$ to $|\eta| < 2$. More importantly, the high $\eta$ leptons and photons provide opportunities for previously inaccessible physics. The high $\eta$ leptons are very sensitive to physics in the small $x$ region, and the high $\eta$ leptons and photons are essential to observe the radiation zero in the $W\gamma$ production (see Section 2.4.5).

It is therefore important to preserve the tracking capability to high $\eta$. The COT tracking efficiency falls off rapidly beyond $|\eta| \sim 1$. The replacement of the radiation-damaged SVXII with a new silicon detector will maintain tracking capability at high $\eta$.

#### 2.4.2.2 Muons

Concerns about the aging and inefficiency of the CSX central muon scintillators have prompted their study and the proposal to eventually replace these counters. These counters are important for triggering and timing of muons and are therefore very important for the electroweak physics goals of Run IIb.

#### 2.4.2.3 Photons

Cosmic rays are a significant background for analyses involving photons and/or $\not\!\!E_T$ , such as studies of diboson production. Most electromagnetic showers produced by cosmic rays are out-of-time with the beam crossing. The proposed Run IIb upgrade to add timing information to the electromagnetic calorimeter would significantly reduce the cosmic ray back-

| channel | | number of events $\int Ldt = 2$/fb | number of events $\int Ldt = 15$/fb |
|---|---|---|---|
| $W \to e\nu$ | $(e^c)$ | 1,120,000 | 8,400,000 |
| $W \to e\nu$ | $(e^p)$ | 448,000 | 3,360,000 |
| $W \to \mu\nu$ | $(\mu^c)$ | 672,000 | 5,040,000 |
| $W \to \mu\nu$ | $(\mu^f)$ | 49,000 | 368,000 |
| $Z \to ee$ | $(e^c, e^{c,p,f})$ | 146,000 | 1,095,000 |
| $Z \to \mu\mu$ | $(\mu^c, \mu^c)$ | 56,000 | 420,000 |
| $W\gamma$, $E_T^\gamma > 10$ GeV | $(\gamma^{c,p})$ | 1,700 | 12,750 |
| $Z\gamma$, $E_T^\gamma > 10$ GeV | $(\gamma^{c,p})$ | 509 | 3,818 |
| $WW \to \ell\nu\ell\nu$ | | 90 | 675 |
| $WZ \to \ell\nu\ell\ell$ | | 12 | 90 |
| $ZZ \to \ell\ell\ell\ell$ | | 1.4 | 10 |
| $WZ \to \ell\nu b\bar{b}$ | | 4 | 30 |
| $ZZ \to \ell\ell b\bar{b}$ | | 0.5 | 3 |

Table 2.5: Expected $W$, $Z$, and diboson event yields with 2 fb$^{-1}$ and 15 fb$^{-1}$ when the Run Ib configuration is assumed. $c$, $p$, and $f$ for electrons represent Run I CEM, PEM, and FEM, and $c$ and $f$ for muons represent Run I CMU/P and FMU.

ground and have a big impact on the sensitivity in diboson analyses. This is exemplified by the $Z\gamma$ coupling measurements in the powerful $Z\gamma \to \nu\nu\gamma$ channel, where photon identification is of paramount importance. With improved photon identification, this channel will become available to CDF in Run IIb.

### 2.4.3 W Mass

The mass of the $W$ boson is a fundamental parameter of the Standard Model. A direct measurement of $M_W$ can be compared with the prediction from other LEP and SLC results as a test of the SM. In the context of other precise electroweak measurements, direct and precise measurements of $M_W$ and $M_{\rm top}$ provide an indirect constraint on the Higgs boson mass, $M_H$, via electroweak radiative corrections. The ultimate test of the SM may lie in the comparison of this indirect determination of $M_H$ with its direct observation.

At the Tevatron, the $W$ mass is extracted from a fit to the $W$ transverse mass, $M_T^W$, and the lepton $p_T$ distributions. The 4 pb$^{-1}$ of the 1988-89 Tevatron Collider run enabled CDF to measure the $W$ mass to be

$$M_W = 79.91 \pm 0.39 \text{ GeV/c}^2 \text{ [6]},$$

and with 19 pb$^{-1}$ from Run Ia CDF measured

$$M_W = 80.41 \pm 0.18 \text{ GeV/c}^2 \text{ [7]}.$$

With 85 pb$^{-1}$ from Run Ib CDF measured

$$M_W = 80.470 \pm 0.089 \text{ GeV/c}^2 \text{ [8]}.$$

The uncertainties in the current Run Ib measurement scale rather well with statistics from the previous measurements; while the difficulty of the measurement has increased, no systematic limitation is yet evident. The fits to the data from Run Ib are shown in Figure 2.21. The uncertainties for the Run Ib measurement are shown in Table 2.6.

Figure 2.20 ($a$) shows the sensitivity in the $M_W$-$M_{\rm top}$ plane of the combined CDF $W$ mass measurement of $M_W = 80.433 \pm 0.079$ GeV/c$^2$ [8] and the top mass measurement $M_{\rm top} = 176.1 \pm 6.6$ GeV/c$^2$ [5], compared to theoretical predictions based on electroweak radiative corrections [2].

In the Run IIa TDR we made a case that a data set of 2 fb$^{-1}$ will allow CDF II to measure the $W$ mass to $\pm 40$ MeV/c$^2$, which is comparable to the overall LEP2 expectation ($\sim$ 40 MeV). Figure 2.20 shows the sensitivity in the $M_W$-$M_{\rm top}$ plane of this estimate when combined with the expected precision $\delta M_{\rm top} = 4$ GeV/c$^2$ for the same dataset. With a dataset of 15 fb$^{-1}$, we make the case below that $\delta M_W = 20$ MeV/c$^2$ (and $\delta M_{\rm top} = 2$ GeV/c$^2$) is within reach. The precision measurement of the W boson and top quark mass with CDF IIb will allow inference of the Standard Model Higgs boson mass

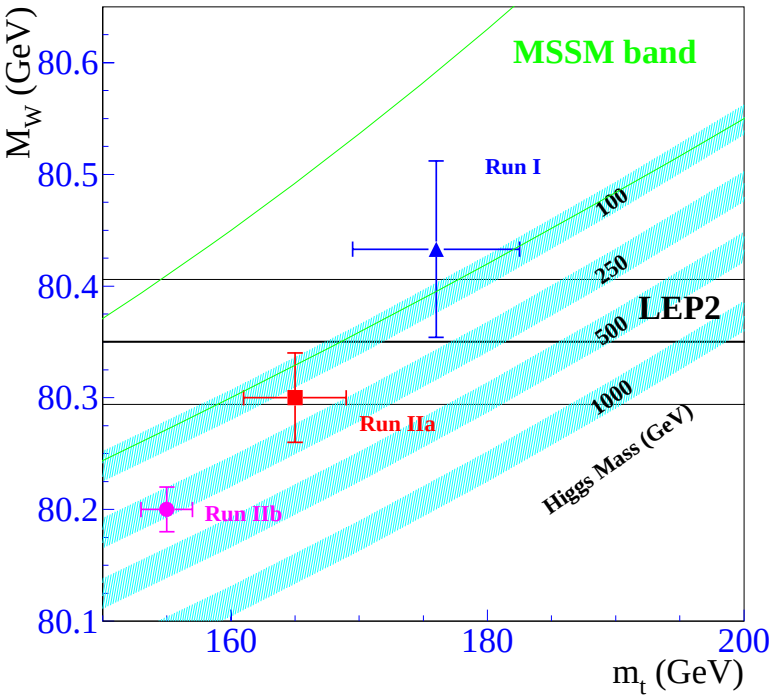


Figure 2.20: The data point labeled "Run I" represents the CDF measurements of $M_W$ and $M_{\rm top}$, and the points labeled "Run IIa" and Run IIb" represent the CDF II estimates for 2 fb$^{-1}$ and 15 fb$^{-1}$. The curves are from a calculation [2] of the dependence of $M_W$ on $M_{\rm top}$ in the minimal standard model using several Higgs masses. The bands are the uncertainties obtained by folding in quadrature uncertainties on $\alpha(M_Z^2)$, $M_Z$, and $\alpha_s(M_Z^2)$. Also indicated is the calculation based on a minimal supersymmetric extension of the standard model (MSSM) [9].

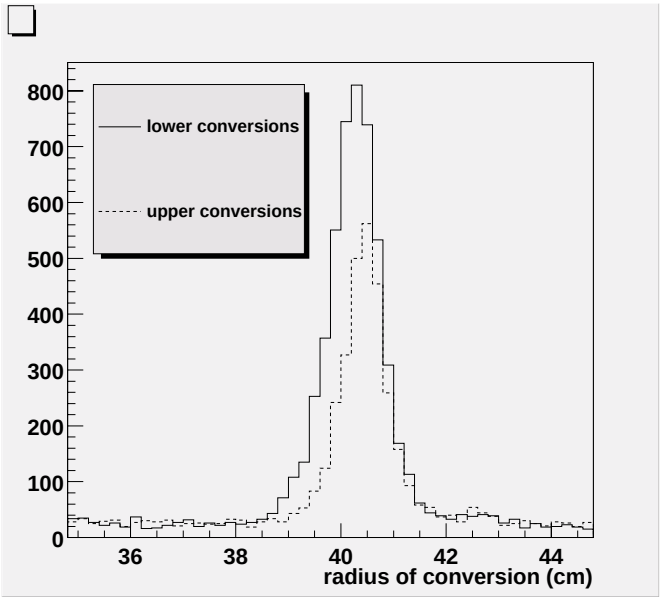


Figure 2.22: The radial distributions for conversions from the Run II commissioning run, in the vicinity of the COT inner wall. An aluminum radiator was attached to the inside of the COT wall on the lower side for calibration.

with an uncertainty of $\delta M_H/M_H \sim 30\%$, assuming we will not be limited by the uncertainty in $\alpha(M_Z)$.

For Run II, the statistical uncertainty and most of systematic uncertainties are expected to be reduced significantly compared to Run I. A salient feature of the $W$ mass analyses has been that most of the inputs required for the measurement have been constrained from the collider data. Thus we believe that, with a factor of 7.5 more data, a reduction of the total uncertainty by a factor of 2 is feasible and includes some conservatism. The individual uncertainties are briefly discussed.

#### 2.4.3.1 Statistical Uncertainty

For Run Ib the typical instantaneous luminosity at the beginning of runs was about $2 \times 10^{31}$ cm$^{-2}$ sec$^{-1}$ and we had about 2.5 extra minimum bias events overlying $W$ and $Z$ events on average. This results in about a 10% loss in statistical precision due to the degraded resolution in the recoil measurement in Run Ib as opposed to Run Ia. For 132 ns operation in Run II the increased number of bunches will more than compensate for the higher luminosity and the number of extra minimum bias events will be to the Run Ia level. This will give us a situation which is better than Run Ib in terms of the statistical power of the data.

#### 2.4.3.2 Track momentum scale and resolution

**Scale:** Knowledge of material in the tracking volume is of importance in determining the momentum and energy scale. The associated systematics are the uncertainties in the muon energy loss ($dE/dx$) for the momentum scale and in the radiative shift of the electron $E/p$ peak for the energy scale. Although the amount of material in the tracking volume will be changed we have shown that photon conversions allow us to measure the amount of material in radiation length quite accurately, as illustrated in Figure 2.22 and can reduce the uncertainties on the $W$ mass mea-

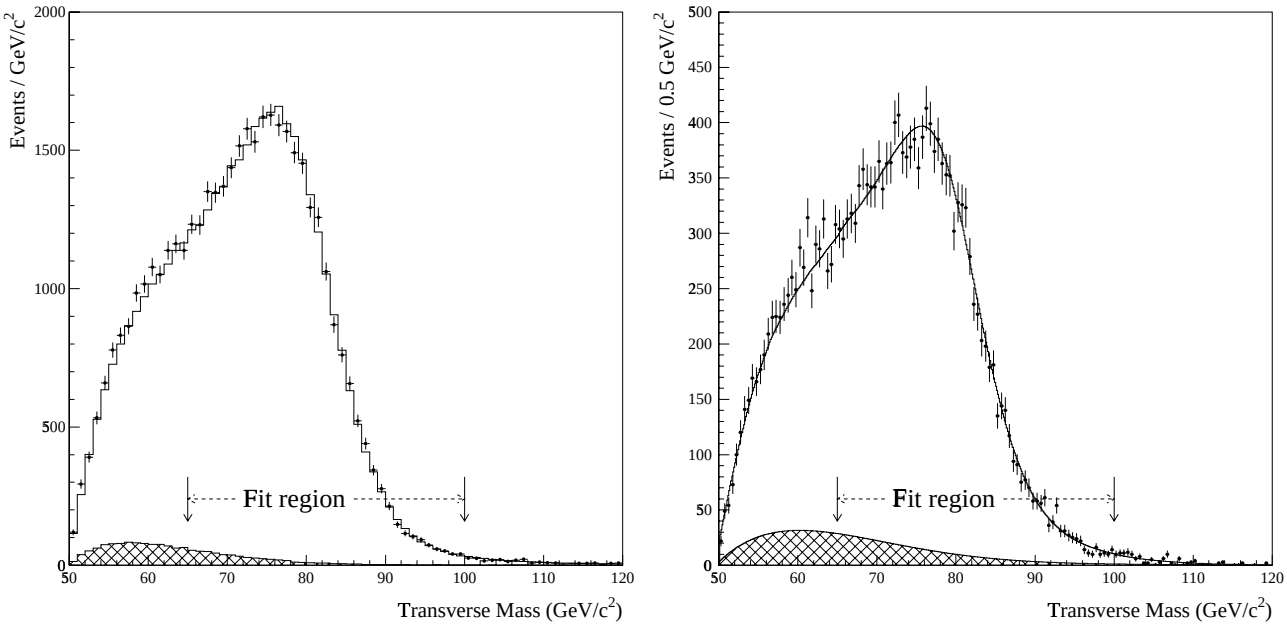


Figure 2.21: Transverse mass distributions and fits for $W \to e\nu$ (left) and $W \to \mu\nu$ (right) from Run Ib.

| Source | $W \to e\nu$ | $W \to \mu\nu$ | common |
|---|---|---|---|
| statistical | 65 | 100 | |
| lepton scale | 75 | 85 | |
| lepton resolution | 25 | 20 | |
| pdfs | 15 | 15 | 15 |
| $p_T^W$ | 15 | 20 | 3 |
| recoil | 37 | 35 | |
| higher order QED | 20 | 10 | 5 |
| trigger, lepton identification bias | - | $15 \oplus 10$ | |
| backgrounds | 5 | 25 | |
| total | 92 | 103 | 16 |

Table 2.6: Systematic uncertainties in the $W$ mass (in MeV) in the CDF measurements from the Run 1B data.

| Source of Uncertainty | Uncertainty (MeV/c$^2$) | | |
|---|---|---|---|
| | $W \to e\nu$ | $W \to \mu\nu$ | Common |
| Statistical | 5 | 8 | – |
| Lepton Energy/Momentum Scale | 10 | 8 | 8 |
| Lepton Energy/Momentum Resolution | 4 | 3 | – |
| Recoil modeling | 3 | 3 | 3 |
| Trigger, Event Selection | 5 | 5 | – |
| Backgrounds | 5 | 5 | – |
| $p_T^W$ | 5 | 5 | 5 |
| PDF | 5 | 5 | 5 |
| QED radiative corrections | 5 | 5 | 5 |
| Total Uncertainty | 17 | 17 | 12 |
| $e$ and $\mu$ Combined Uncertainty | | 15 | |

Table 2.7: Estimates of uncertainties in the $W$ mass measurement for 15 fb$^{-1}$.

surement. During the commissioning run for Run IIa, a precisely-known aluminum radiator was placed inside the COT inner wall to provide a calibration reference using conversions.

The $dE/dx$ muon energy loss requires information of the material type in addition to the radiation length. For example, an unknown type of 1% $X_o$ material leads to about 10 MeV uncertainty in the $W$ mass measurement. We have fairly detailed information available on the construction of the Run IIa tracking detectors and do not expect this to be a limitation.

**Resolution:** It is important to assess the impact of high luminosity running on the track momentum resolution. In Run Ib, the CTC track resolution degraded with luminosity, but could be recovered when SVX hits or the SVX beam position were added to the tracking. For instance, if we compare early Run Ib ($\mathcal{L} \sim 0.2 \times 10^{31}$) to later Run Ib ($\mathcal{L} \sim 1 \times 10^{31}$), the CTC track resolution observed in the width of the $J/\psi$ peak worsens by 35%, but the SVX + CTC track resolution worsens by only 10%. The new tracking system incorporates this linking naturally across all detectors (for $|\eta| \leq 1.0$). It is clearly important here to maintain the tracking capability of the Run IIa SVXII-ISL-COT integrated system.

The $M_W$ uncertainty due to the momentum resolution uncertainty will scale with statistics since the resolution is determined using $Z \to \mu\mu$ events.

#### 2.4.3.3 Calorimeter energy scale and resolution

The dominant uncertainty in the electron energy scale for Run I was from the uncertainty in amount of material in radiation length, and statistics. As described above, the amount of material is expected to be well measured by photon conversion events for Run IIb and the uncertainty should scale with statistics.

The $M_W$ uncertainty due to the energy resolution uncertainty will scale with statistics since the resolution is determined using $Z \to ee$ events.

#### 2.4.3.4 Recoiling energy modeling

The detector response to the recoil energy against $W$ is directly calibrated using $Z \to ee$. Therefore the uncertainty will scale with statistics. For Run II with the muon coverage at high $\eta$, $Z \to \mu\mu$ can also be used.

#### 2.4.3.5 $W$ Production model

$P_T^W$ : For the $P_T^W$ spectrum, the $P_T^Z$ distribution from $ee, \mu\mu$ and a new theoretical calculation which includes soft gluon resummation effects and $W$, $Z$ decays are expected to provide appropriate checks and improved theoretical guidance, and will allow the reduction of the current uncertainty in $M_W$ substantially.

The Run I measurement of $d\sigma/dP_T^Z$ [10] is shown in

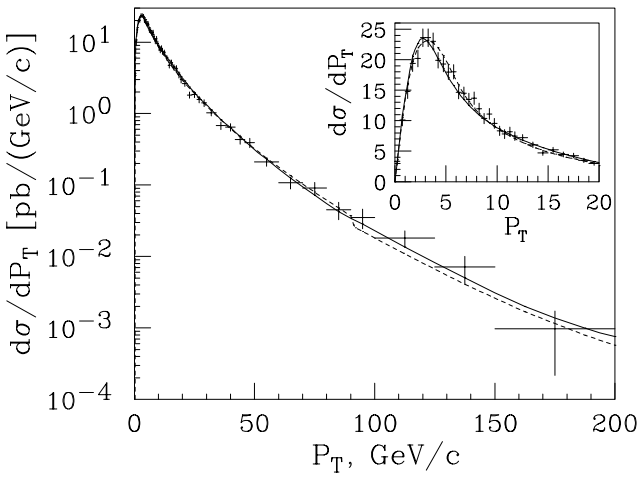


Figure 2.23: The $d\sigma/dp_T$ of $e^+e^-$ pairs in the mass range $66-116$ GeV/c$^2$. The inset shows the $p_T < 20$ GeV/c region with a linear ordinate. The crosses are the data with all errors included, except the 3.9% luminosity error. The dashed (solid) curve is the EV ($Z$-only RESBOS) prediction with the cross section normalized to 248 pb.

Fig. 2.23. With 15 fb$^{-1}$ of Run IIb data, the errors in the low $P_T^Z$ region are expected to be 1%, providing a very strong constraint on the theoretical model in the region relevant for the $W$ mass measurement.

**Parton Distribution Functions**: The Run I uncertainty in PDF's was constrained by the CDF $W$ asymmetry measurement (see Figure 2.24), which will become more precise with statistics. Forward coverage is very important for this measurement since the PDF sensitivity increases with the rapidity coverage. The data in the central region probes the $d$ and $u$ distributions in the $x$ region between 0.02 and 0.15. The forward data probes the region between 0.006 (a new region of $x$) and 0.35.

However, Monte Carlo studies have shown that the $W$ charge asymmetry does not have the same sensitivity to all aspects of the PDF's as the $W$ mass measurement. Therefore additional measurements are likely to be needed which will constrain PDF's in different ways. The $y$ distributions of $Z$ ($y_Z$) from dileptons have sensitivity to constrain PDFs, and this may help reducing the PDF uncertainty in $M_W$. A precise measurement of $Z$ efficiency as a function $y_Z$ in a wide rapidity region is required, which can be measured using the $Z$ sample itself with sufficient statistics. Figure 2.25 shows the Run I measurement [11] of $d\sigma/dy$ for Drell-Yan production. The measurement is completely limited by statistics in Run I, and is likely to remain so even beyond 2 fb$^{-1}$. For this measurement forward coverage is essential. Similar but additional information on PDF's can be obtained by measuring the lepton rapidity distribution in $W$ decays.

Cross section measurements of Drell-Yan production [12] (especially the low mass region) can be used to get further constraints on PDFs. The Run I Drell-Yan cross section measurements using central electrons are shown in Figure 2.26. The low mass data is sensitive to the very low $x$ region. Run IIb upgrades to the DAQ bandwidth will be important for this program in order to preserve our ability to trigger on low $p_T$ lepton pairs.

The PDF uncertainty can also be reduced by raising the minimum $M_T^W$ for fitting. This will imply a larger statistical uncertainty, and is an example of using the huge Run IIb statistics to reduce systematics and the total uncertainty.

While the PDF uncertainty will warrant attention, it is likely that a program of measurements with collider data will prevent it from dominating the $W$ mass measurement. It should be noted that the combined D run I measurement, including the forward calorimeter data, already quotes a PDF uncertainty of 7 MeV [13].

**QCD higher order corrections** : The effects of higher-order QCD corrections on the $W$ polarization have been calculated at $O(\alpha_s^2)$. The $W$ mass is measured using the low $p_T^W$ sample where the higher order QCD corrections are modest. The uncertainty is negligible in current analyses, and should not be a fundamental problem in the future. This effect has been measured in Run I [14] and the measurement is statistically limited. With Run IIb statistics, a precise measurement of the $W$ polarization as a function of $p_T^W$ will be possible.

**QED Radiative corrections** : Radiative corrections in $M_W$ are rather large: the shifts in $M_W$ due to the final state radiation are 65 MeV in the $W \to e\nu$ channel and 168 MeV in the $W \to \mu\nu$ channel. For Run Ib, the uncertainty in these shifts due to missing diagrams was estimated to be 20 MeV and 10 MeV for the electron and muon channels respectively. Recently, a more thorough calculation [15] of electroweak radiative $W$ and $Z$ boson production and decay, in-

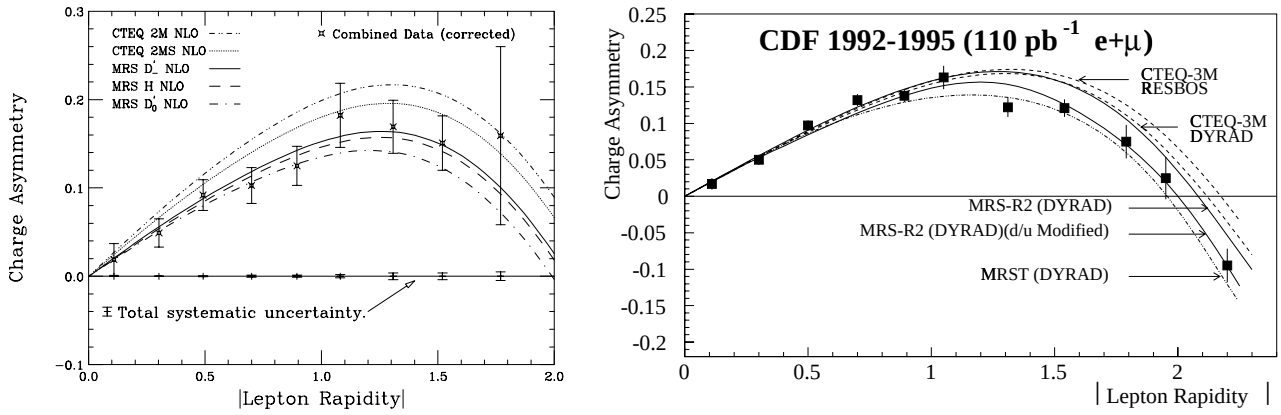


Figure 2.24: Left: Combined Run Ia $W$ charge asymmetry measurement using muons and central and plug electrons. Right: Combined $W$ charge asymmetry using Run Ia and Ib data including the forward muons, showing the effect of the larger rapidity coverage and higher statistics.

cluding initial and final state radiation, finite lepton masses, and finite $W$, $Z$ width effects. A two-photon calculation is also available [16]. This will make it possible to reduce the error associated with radiative corrections substantially in the future.

#### 2.4.3.6 Backgrounds

The $Z \to \mu\mu$ background (one muon in the central muon chambers and the other muon in high $\eta$ region) in the $W \to \mu\nu$ sample is the dominant background for this channel and its uncertainty derives from the choice of PDF's and the tracking efficiency at high $\eta$. For Run II, the tracking upgrade (well measured ISL+SVXII tracks in the region $1 < |\eta| < 2$) and the forward muon upgrade (muons in the region $1.5 < |\eta| < 3$) together with the muon signature in the plug upgrade calorimeter will remove most of this background and will reduce the uncertainty. This uncertainty does not scale easily with statistics, but forward tracking and muon coverage is clearly very important to control this source of background.

#### 2.4.3.7 Trigger and Selection Bias

For Run Ib, there was a 15 MeV uncertainty due to a possible momentum dependence of the muon triggers in the $W \to \mu\nu$ channel. The measurement of the momentum dependence was statistically limited. The muon selection is also possibly affected by the presence of nearby jets.

For Run IIb, it is important to maintain unbiased triggers. That is, the momentum thresholds should be low enough not to introduce a $P_T$ or $E_T$ dependence above 25 GeV. Also, the lepton selection should not be biased by hadronic activity. This means we must maintain high tracking efficiency as the luminosity increases.

#### 2.4.3.8 $W$ mass summary

We make a conservative estimate that 15 fb$^{-1}$ will allow CDF II to measure the $W$ mass to $\pm 20$ MeV/c$^2$, which will be a significant improvement over the Run IIa measurement and the world average, giving the Tevatron the leading role in the measurement of this important parameter. Coupled with a commensurate improvement in the top mass precision, this will give the Tevatron the dominant position in constraining the Higgs mass. The estimates of individual uncertainties is shown in Table 2.7.

### 2.4.4 $W$ Width

The leptonic branching ratio of the $W$ may be inferred from the ratio $R = \sigma \cdot Br(W \to l\nu)/\sigma \cdot Br(Z \to ll)$, using LEP measurements for the $Z$ couplings and a theoretical prediction of the production cross section ratio. It provides a standard model consistency check. For Run Ia [17] CDF measured $Br(W \to e\nu) = 0.109 \pm 0.0033(\text{stat}) \pm 0.0031(\text{syst})$. If one further assumes standard couplings for $W \to e\nu$, one can derive a value for the total width of the $W$ boson, $\Gamma_W = 2.064 \pm 0.0060(\text{stat}) \pm 0.0059(\text{syst})$ GeV. The theoretical uncertainty in the cross section ratio is expected to limit precision to about $\pm 1\%$. How-

ever, the upgraded momentum measurement in the region $1 < |\eta| < 2$ should give improved acceptance systematics, reducing the dependence on the parton distribution functions.

The $W$ width can be measured directly from the shape of the transverse mass distribution (see Figure 2.27). For $M_T^W > 100$ GeV/c$^2$ resolution effects are under control and using Run Ib in the modes $W \to e\nu$ and $W \to \mu\nu$, CDF measured $\Gamma_W = 2.04 \pm 0.11(\text{stat}) \pm 0.09(\text{syst})$ GeV [19]. The direct measurement of the $W$ width closely follows the measurement of the $W$ mass. The uncertainties will likely scale with statistics allowing a $\pm 15$ MeV measurement for 15 fb$^{-1}$, much better than the LEP2 expectation of $\pm 200$ MeV, and providing a stringent test of the standard model.

### 2.4.5 Gauge Boson Couplings

The Standard Model makes specific predictions for the trilinear couplings of the gauge bosons, $W$, $Z$, and $\gamma$. The nature of these couplings can be investigated via studies of $W\gamma$ and $Z\gamma$ production [20] and $WW$, $WZ$ and $ZZ$ pair production [21]. The major goals of these studies will be testing the Standard Model prediction(s) and searching for new physics. The Run I results are summarized in Table 2.8 (see also [3] for details).

$W\gamma$ production in $p\bar{p}$ collisions is of special interest due to the SM prediction of a radiation amplitude zero in the charge-signed $Q_W \cdot \cos\theta^*_\gamma$ distribution at $\sim -0.3$. The radiation zero is also predicted to manifest itself as a "channel" in the charge-signed $Q_W\eta_\ell$ *vs.* $Q_W\eta_\gamma$ 2-dimensional distribution [22], and as a strong "dip" in the charge-signed photon-$W$ decay lepton rapidity difference distribution, $Q_W \cdot (\eta_\gamma - \eta_\ell)$ at $\sim -0.3$.

By using central and plug electrons and photons, it will be possible in Run IIa to conclusively establish the dip in the photon lepton rapidity difference distribution. On the other hand, for central electrons and photons only, the dip is not statistically significant with Run IIa statistics and will benefit from Run IIb statistics. Also, the increased statistics will help to measure the location of the dip more precisely and provide a better test of the standard model prediction.

Backgrounds from electromagnetic showers induced by cosmic rays are important for diboson analyses. For example, a $W \to e\nu$ event with a cosmic ray would look like a $W\gamma$ event with anomalous $\not\!\!E_T$ . Similarly, a $Z \to ee$ event with an overlapping cosmic ray would give an $ee\gamma\not\!\!E_T$ signature. The process $p\bar{p} \to Z^0(\to \nu\bar{\nu}) + \gamma + X$ has large cosmic ray backgrounds. Sensitivity to $Z\gamma$ anomalous couplings is statistics-limited and this channel has the advantage over the $\ell^+\ell^-\gamma$ channel by a factor of 3 in the branching ratio, and almost a factor of 2 in the acceptance. The D experiment has taken advantage of its pointing calorimeter to control cosmic ray backgrounds, and has produced the best $Z\gamma$ measurement by using the $\gamma\not\!\!E_T$ channel [23]. By using the EM calorimeter timing information provided by the proposed Run IIb upgrade, the cosmic ray background can be controlled much better and the sensitivity of these diboson analyses will increase significantly.

For Run II, we anticipate that the current results from CDF will undergo further significant improvements with 15 fb$^{-1}$ integrated luminosity, in conjunction with the Run II upgrades of the overall tracking, calorimeter, muon and DAQ systems. Since the acceptance for diboson events increases rapidly with rapidity coverage, it is important to maintain this capability through Run IIb to fully exploit the increased luminosity. The sensitivity for $WWV$ and $ZZ\gamma$ anomalous coupling is limited by the statistics of backgrounds and potential signal and therefore benefits from larger data sizes, improving as $N^{1/4}$. The CDF IIb measurements with 15 fb$^{-1}$ (see Table 2.9) are anticipated to surpass those from LEP-II experiments. The Tevatron also has a significant advantage over LEP-II because the Tevatron can produce all the three ($W\gamma$, $WW$ and $WZ$) final states and therefore obtain independent sensitivity to the different couplings with fewer assumptions.

In addition to the increased sensitivity to anomalous couplings through potential excesses in the data, 15 fb$^{-1}$ of integrated luminosity makes it possible to *measure* all the diboson production cross sections with good precision. This is particularly true for the $WW$, $WZ$ and $ZZ$ cross sections which are statistically limited even with 15 fb$^{-1}$ (see Table 2.5). The precise measurements of these cross sections means that we will also be sensitive to *deficits* compared to the predicted cross sections. This will add a whole new dimension to diboson physics and new physics searches, which makes a strong case for going beyond 2 fb$^{-1}$ and acquiring 15 fb$^{-1}$ of data.

The statistics of Run IIb will also make possible for the first time a study of two new diboson channels, $WZ \to l\nu b\bar{b}$ and the $ZZ$ final state. The former chan-

| Mode ($\ell = e, \mu$) | Luminosity ($\text{pb}^{-1}$) | Anomalous Coupling limit (95% C.L.) |
|---|---|---|
| $W\gamma \to \ell\nu, \gamma$ | 20 | $-0.7 \leq \lambda \leq 0.7$, $-2.2 \leq \Delta\kappa \leq 2.3$ |
| $WW \to$ dilepton | 108 | $-0.9 \leq \lambda \leq 0.9$, $-1.0 \leq \Delta\kappa \leq 1.3$ |
| $WW$ and $WZ \to$ leptons + jets | 19.6 | $-0.81 \leq \lambda \leq 0.84$, $-1.11 \leq \Delta\kappa \leq 1.27$ |
| $Z \to \ell\ell\gamma$ | 20 | $-3.0 \leq h_{30}^{Z} \leq 3.0$, $-0.7 \leq h_{40}^{Z} \leq 0.7$ |

Table 2.8: 95% C.L. Anomalous gauge boson coupling limits achieved in Run I analyses by the CDF Collaboration.

| Mode | Luminosity ($\text{fb}^{-1}$) | Anomalous Coupling limit (95% C.L.) |
|---|---|---|
| Combined $W\gamma, WW$ and $WZ$ | 2 | $-0.086 \leq \lambda \leq 0.090$, $-0.12 \leq \Delta\kappa \leq 0.19$ |
| Combined $W\gamma, WW$ and $WZ$ | 15 | $-0.052 \leq \lambda \leq 0.054$, $-0.073 \leq \Delta\kappa \leq 0.115$ |
| $Z\gamma \to ll\gamma$ | 15 | $-0.045 \leq h_{30}^{Z} \leq 0.045$, $-0.0027 \leq h_{40}^{Z} \leq 0.0027$ |
| $Z\gamma \to \nu\nu\gamma$ | 15 | $-0.019 \leq h_{30}^{Z} \leq 0.019$, $-0.0014 \leq h_{40}^{Z} \leq 0.0014$ |

Table 2.9: 95% C.L. Anomalous gauge boson coupling limits that might be achieved in run IIb.

nel is very important to understand as a background to the $WH$ channel for the Higgs search.

### 2.4.6 Forward-Backward $Z$ Asymmetry

The presence of both vector and axial-vector couplings of electroweak bosons to fermions in the process $q\bar{q} \to Z^0/\gamma \to e^+e^-$ gives rise to an angular asymmetry, "Forward-Backward Asymmetry", in the emission angle of the electron in the rest frame of the electron-positron pair. This asymmetry, $A_{FB}$, is a direct probe of the relative strengths of the vector and axial-vector couplings over the range of $Q^2$ being considered. In addition, $A_{FB}$ constrains the properties of any hypothetical heavy neutral gauge bosons not included in the Standard Model. For values of $Q^2$ significantly larger than $M_Z^2$, $A_{FB}$ is predicted to be large and positive (approximately 0.5), which makes it sensitive to deviations induced by new physics.

From $\sim$110 $\text{pb}^{-1}$ of the Run I dielectron data, CDF has measured[24] $A_{FB}$ to be $0.070 \pm 0.016$ using a sample of 5463 events in the $Z$ pole region defined by $75 < M_{ee} < 105$ GeV, and $0.43 \pm 0.10$ using a sample of 183 events in the high mass region defined by $M_{ee} > 105$ GeV. These measurements can be compared with the Standard Model predictions of $0.052 \pm 0.002$ and $0.528 \pm 0.009$. Table 2.10 summarizes our measured values for $A_{FB}$ and its uncertainties in both invariant mass regions. The statistical errors are dominant, and the sources of systematic uncertainty (from background level determination and electron pair mass resolution) are expected to scale with statistics as well. This means that these measurements will benefit from increased statistics even beyond 15 $\text{fb}^{-1}$.

In the vicinity of the $Z^0$ pole it will be possible to extract a precision measurement of $\sin^2\theta_W^{eff}$ from $A_{FB}$. The uncertainty in $\sin^2\theta_W^{eff}$ should also scale with statistics since $A_{FB}$ is proportional to $(\sin^2\theta_W^{eff} - 0.25)$. Under the assumption that all uncertainties scale with statistics, we expect an uncertainty in $A_{FB}$ of 0.001 and an uncertainty in $\sin^2\theta_W^{eff}$ of 0.0004 with 15 $\text{fb}^{-1}$. The theoretical uncertainty in $A_{FB}$ due to parton distribution uncertainty should be below 0.001, and with further improvements in PDF's should not pose a limitation.

It should be noted that if $\sin^2\theta_W^{eff}$ is measured to within 0.0004 as expected, then the CDF IIb result will improve upon the LEP I and SLD results which measure $\sin^2\theta_W^{eff}$ from jet charge asymmetries in hadronic $Z^0$ decays with an uncertainty of $\sim 0.001$. Since the initial and final states are reversed in the two cases, the systematics are also different.

Well above the $Z^0$ pole, for electron pairs with invariant mass in excess of 105 $\text{GeV/c}^2$, $A_{FB}$ is dominated by $Z^0/\gamma$ interference, and a large positive value is predicted for $A_{FB}$ with a very flat dependence in

| | $75\ \mathrm{GeV/c^2} < \mathrm{M}_{ee} < 105\ \mathrm{GeV/c^2}$ | | $\mathrm{M}_{ee} > 105\ \mathrm{GeV/c^2}$ | |
|---|---|---|---|---|
| | CC | CP | CC | CP |
| Raw event sample | 2602 | 2861 | 98 | 85 |
| Background | $0^{+2}_{-0}$ | $110 \pm 36$ | $1^{+2}_{-1}$ | $1^{+21}_{-1}$ |
| Predicted Asymmetry | 0.052±0.002 | | 0.528±0.009 | |
| Measured Asymmetry | 0.070±0.016 | | 0.43±0.10 | |
| Uncertainty in $\mathrm{A}_{FB}$ | | | | |
| Statistical | 0.015 | | 0.08 | |
| Background subtraction | 0.002 | | 0.04 | |
| Mass Deconvolution | 0.003 | | 0.03 | |
| Total uncertainty | 0.016 | | 0.10 | |

Table 2.10: Run I ($110\ \mathrm{pb}^{-1}$) measurements of $A_{FB}$.

electron pair invariant mass. There can be strong variations in $\mathrm{A}_{FB}$ with invariant mass due to a variety of exotic physics at higher invariant mass scales, including most Z′ or composite Z models [25], and also lepton compositeness models, exchange of leptoquarks or R-parity violating SUSY particles, and extra dimensions. Moreover, if new physics is discovered at CDF II, $\mathrm{A}_{FB}$ measurements will provide discrimination between various models.

As with the measurements of $\mathrm{A}_{FB}$ at the $\mathrm{Z}^0$ pole, we expect the uncertainty in the measurements above the $\mathrm{Z}^0$ pole to scale with statistics compared to the Run I measurement [24]. For electron pairs with invariant mass between 105 $\mathrm{GeV/c^2}$ and 195 $\mathrm{GeV/c^2}$, we expect to collect approximately 20,000 events with 15 $\mathrm{fb}^{-1}$. Using this entire sample we expect to measure $\mathrm{A}_{FB}$ to within 0.007. For electron pairs with invariant mass above 195 $\mathrm{GeV/c^2}$ (above the LEP 200 maximum $\sqrt{s}$), we expect to collect approximately 2,000 events, which should allow a measurement of $\mathrm{A}_{FB}$ to within 0.025. Parton distribution function uncertainty will not significantly affect this sensitivity.

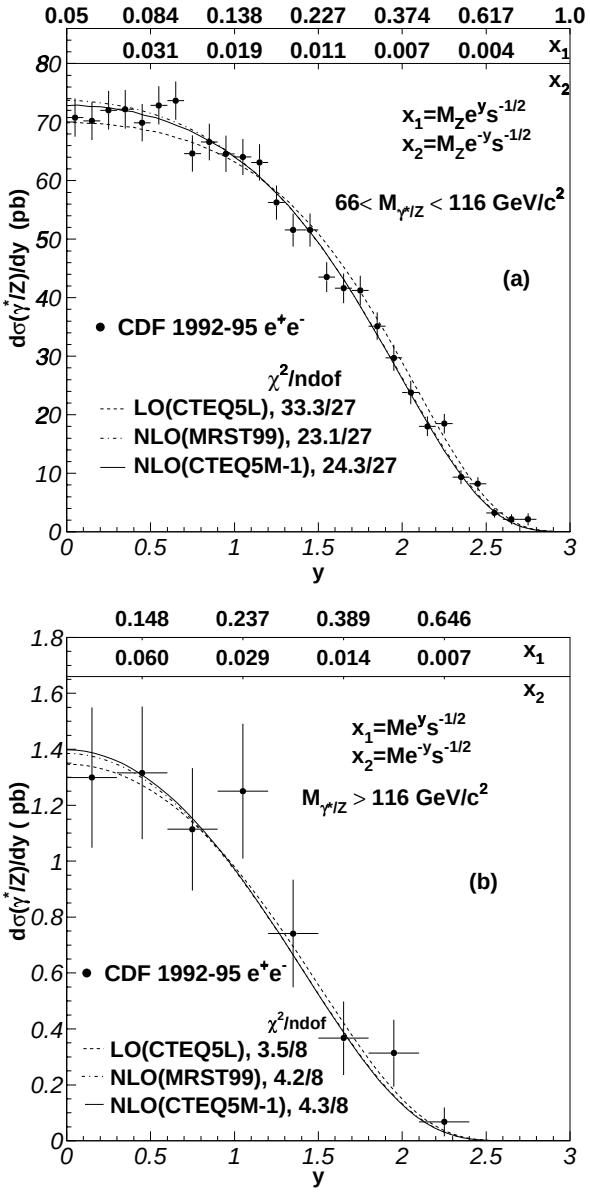


Figure 2.25: $d\sigma/dy$ distributions of $e^+e^-$ pairs in (a) the $Z$ boson mass region, and $b$ the high mass region. The error bars on the data include statistical errors only. The theoretical predictions have been normalized to the data in the $Z$ boson mass region. The top horizontal axes on the figures are the corresponding values of $x_1$ and $x_2$ as a function of $y$. The $M$ used to obtain $x_1$ and $x_2$ in (b) is the mean mass over the bin.

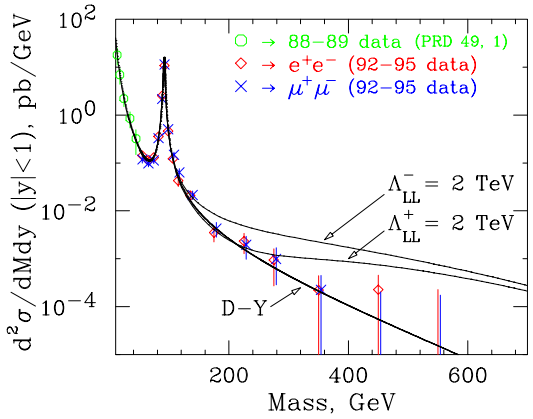


Figure 2.26: Drell-Yan dilepton $(e^+e^-, \mu^+\mu^-)$ production cross section from Run I as a function of the dilepton invariant mass. Also shown are expectations from compositeness models.

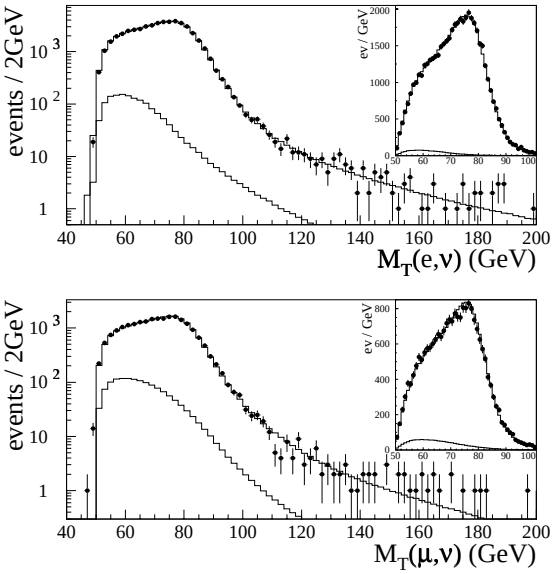


Figure 2.27: Run Ib transverse mass distributions (filled circles) for $W \to e\nu$ (upper) and $W \to \mu\nu$ (lower), with best fit Monte Carlo fits superimposed as a solid curve. The lower curve in each plot shows the sum of the estimated backgrounds. Each inset shows the 50-100 GeV region on a linear scale.

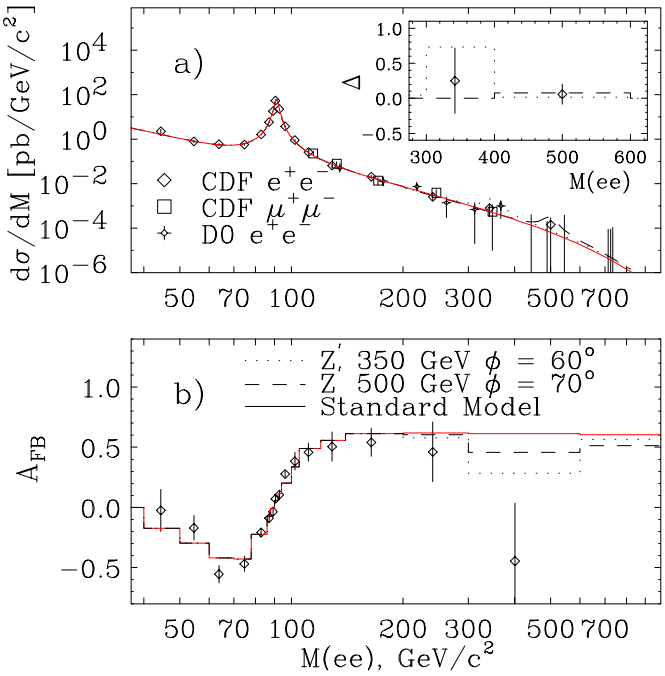


Figure 2.28: (a) $d\sigma/dM$ distribution of $e^+e^-$ and $\mu^+\mu^-$ pairs. All errors (except for the overall 3.9% luminosity error) have been combined in quadrature. The standard model theoretical predictions (solid lines) have been normalized to the data in the $Z$ boson mass region. Also shown are the $e^+e^-$ measurements from D. (b) $A_{FB}$ versus mass compared to the standard model expectation (solid line). Also, predicted theoretical curves for $d\sigma/dM$ and $A_{FB}$ with an extra $E_6$ $Z'$ boson (width of 10%) with $M_{Z'} = 350$ GeV (dotted line) and 500 GeV (dashed line). The inset in (a) shows the difference, "$\Delta$" in fb/GeV/c$^2$, between the CDF $e^+e^-$ $d\sigma/dM$ data and the standard model prediction (on a linear scale) compared to the expectation from these two $Z'$ models.

# Bibliography


[1] S. L. Glashow, Nucl. Phys. **22**, 579 (1961); S. Weinberg, Phys. Rev. Lett. **19**, 1264 (1967); A. Salam, in *Elementary Particle Theory: Relativistic Groups and Analyticity*, ed. N. Svartholm (Almqvist and Wiksell, Stockholm, 1968), p. 367.

[2] G. Degrassi *et al.* Phys. Lett. B **418**, 209 (1998); G. Degrassi, P. Gambino, and A. Sirlin, Phys. Lett. B **394**, 188 (1997).

[3] Summary Report of the Fermilab Workshop on QCD and Weak Boson Physics in Run II, Fermilab-Pub-00/297, November 2000.

[4] R. Thurman-Keup, A. V. Kotwal, M. Tecchio and A. Byon-Wagner, Rev. Mod. Phys. 73, 267 (2001).

[5] T. Affolder *et al.* (CDF Collaboration), Phys. Rev. D **63**, 032003 (2001); B. Abbott *et al.* (D0 Collaboration), Phys. Rev. D **60**, 052001 (1999).

[6] F. Abe *et al.*(CDF), Phys. Rev. **D43**, 2070 (1991).

[7] F. Abe *et al.*(CDF), Phys. Rev. Lett. **75**, 11, (1995); Phys. Rev. **D52**, 4784 (1995).

[8] T. Affolder *et al.*(CDF), Phys. Rev. **D64**, 052001 (2001).

[9] P. Chankowski *et al.*, Nucl. Phys. **B417**, 101 (1994); D. Garcia and J. Sola, Mod. Phys. Lett. A **9**, 211 (1994); A. Dabelstein, W. Hollik and W. Mosle, in *Perspectives for Electroweak Interactions in $e^+e^-$ Collisions*, ed. by B. A. Kniehl (World Scientific, Singapore, 1995) p. 345; D. Pierce *et al.*, Nucl. Phys. **B491**, 3 (1997).

[10] T. Affolder *et al.* (CDF), Phys. Rev. Lett. **84**, 845 (2000).

[11] T. Affolder *et al.*(CDF), Phys. Rev. **D63** 011101 (2001).

[12] F. Abe *et al.*(CDF), Phys. Rev. **D49**, R1 (1994).

[13] B. Abbott *et al.*(D), Phys. Rev. Lett. **84**, 222 (2000); Phys. Rev. **D62**, 092006 (2000).

[14] B. Abbott *et al.*(D), Phys. Rev. **D63**, 072001 (2001).

[15] U. Baur, S. Keller and D. Wackeroth, Phys. Rev. **D59**, 013002 (1999).

[16] U. Baur and T. Stelzer, Phys. Rev. **D61**, 073007 (2000).

[17] F. Abe *et al.*(CDF), Phys. Rev. Lett. **73**, 220 (1994).

[18] F. Abe *et al.*(CDF), Phys. Rev. **D50**, 5550 (1994).

[19] T. Affolder *et al.*(CDF), Phys. Rev. Lett. **85**, 3347 (2000).

[20] F. Abe, *et al.*, The CDF Collaboration, Phys. Rev. Lett. **74**, 1936 (1995); F. Abe, *et al.*, The CDF Collaboration, Phys. Rev. Lett. **74**, 1941 (1995).

[21] F. Abe, *et al.*, The CDF Collaboration, Phys. Rev. Lett. **75**, 1017 (1995); F. Abe, *et al.*, The CDF Collaboration, Phys. Rev. Lett. **78**, 4537 (1997).

[22] U. Baur, S. Errede and G. Landsberg, Phys. Rev. D**50**, 1917 (1994).

[23] D Collaboration, S. Abachi *et al.*, Phys. Rev. Lett. **78**, 3640 (1997).

[24] F. Abe *et al.* (CDF), Phys. Rev. Lett. **77**, 2616 (1996); T. Affolder *et al.* (CDF), hep-ex/0106047, submitted to PRL.

[25] J. L. Rosner, Fermilab Report No. FERMILAB-PUB-95/394-T.

[26] F. Abe *et al.*(CDF), Phys. Rev. Lett. **74**, 850 (1995).

## 2.5 Search for New Phenomena

### 2.5.1 Introduction

The Standard Model is widely believed to be incomplete. Indeed, precision electroweak data, combined with the direct search limit from LEP for the Higgs ($H^0$), are moderately inconsistent.[1, 2] Strong theoretical arguments suggest that new physics should emerge at the scale of electroweak symmetry breaking, for example in scenarios invoking supersymmetry, new strong dynamics, or large extra-dimensions.

If we assume that no discoveries are made in the 2 fb$^{-1}$ Run IIa, nevertheless an order of magnitude increase in integrated luminosity will greatly extend the discovery potential of CDF II. This is despite the fact that, as illustrated in Figure 2.29, the reach in mass grows only logarithmically with integrated luminosity. However, numerous models have been suggested that predict new phenomena at a scale accessible at the Tevatron– for example in models of supersymmetry [3, 4, 5, 6, 7, 8], technicolor [9], gauged flavor symmetries[10], and large extra dimensions [11, 12, 13]. However, in many cases small branching ratios for experimentally viable signatures make detection difficult. In this situation one gains as the square-root of the integrated luminosity. Thus, a large discovery potential for CDF II exists in a high-luminosity Tevatron run.

The situation is well illustrated by the case of supersymmetry in a supergravity (SUGRA) scenario. As part of the Physics at Run II Workshop [14], the SUGRA working group studied five choices of SUGRA parameters (for details, see reference [15].) In SUGRA models, charginos and neutralinos tend to be light (100-200 GeV range) and therefore $\tilde{\chi}\tilde{\chi}$ pair production cross sections tend to dominate. This is illustrated in Table 2.11, where $\tilde{\chi}\tilde{\chi}$ production is dominant for all cases except the fourth where there is a large $\tilde{t}$-pair cross section. An effective search strategy in SUGRA models is therefore to look for tri-lepton final states.[19] However, tri-lepton final states, which might arise from three-body decays (e.g. $\tilde{\chi}_1^{\pm} \to \ell\nu_\ell\tilde{\chi}^0$) or leptonic decays of the $\tau$ (particularly in large $\tan\beta$ models such as cases 2,3,5), result in rather small signal cross sections (see Table 2.12). The Standard Model backgrounds from this study are shown in Table 2.13. Whereas with 2 fb$^{-1}$ only case 1 is observable at the $3\sigma$ level in the tri-lepton channel, with 15 fb$^{-1}$ all cases except case 4 are observable at this level in this channel.

Table 2.11: Parameter space choices, sparticle masses and total signal cross sections for the five chosen case studies of the mSUGRA group. The total cross section and fractional contribution to the signal from various subprocesses in the five parameter space cases of reference [15].

| case | (1) | (2) | (3) | (4) | (5) |
|---|---|---|---|---|---|
| $\sigma_{tot}$(fb) | 404 | 653 | 2712 | 3692 | 1393 |
| $\tilde{g},\tilde{q}(\%)$ | 4.3 | 6.6 | 50.4 | 66.2 | 0.01 |
| $\tilde{g}\tilde{\chi},\tilde{q}\tilde{\chi}(\%)$ | 2.4 | 3.6 | 2.9 | 1.2 | 0.01 |
| $\tilde{\chi}\tilde{\chi}(\%)$ | 85.0 | 85 | 45.7 | 32.6 | 99.5 |
| $\tilde{l}\tilde{l}(\%)$ | 8.3 | 4.7 | 1.0 | 0.04 | 0.4 |
| $\tilde{t}\tilde{t}(\%)$ | 1.8 | 1.5 | 41 | 65 | 0.01 |
| $\tilde{\chi}_1^{\pm}\tilde{\chi}_2^0(\%)$ | 43.8 | 45 | 26.5 | 18 | 16.7 |
| $\tilde{\chi}_1^{\pm}\tilde{\chi}_1^{\pm}(\%)$ | 33.5 | 33 | 17.6 | 13 | 24.6 |

Table 2.12: The $3\ell$ signal (fb) in 5 parameter points (adapted from [15]) The lepton $p_T$ thresholds are 11,7, and 5 GeV.

| case | $\sigma$ fb |
|---|---|
| (1) | $7.39 \pm 0.12$ |
| (2) | $0.93 \pm 0.06$ |
| (3) | $1.08 \pm 0.12$ |
| (4) | $2.72 \pm 0.23$ |
| (5) | $0.63 \pm 0.07$ |

An additional analysis was performed for sensitivity in a more general minimal SUGRA model with essentially the same cuts.[15] As shown in Figure 2.30, the reach increases significantly for a high luminosity run (here taken as 30 fb$^{-1}$).

### 2.5.2 Generic exotic signatures and the CDF II upgrade

The search for new phenomena looks for any deviation from Standard Model expectations. However, guided by theory, historical precedent (e.g. high $p_T$ leptons), and sometimes serendipity (e.g. the CDF $ee\gamma\gamma\not\!\!E_T$ candidate event), certain generic signatures emerge: missing transverse momentum($\not\!\!E_T$), high-$p_T$ leptons ($e,\mu$), multi-leptons, high-$p_T$ jets, displaced vertices, high-$p_T$ photons, hadronic $\tau$-decays, and highly-ionizing particles. The CDF upgrade has been designed to detect these objects with precision and

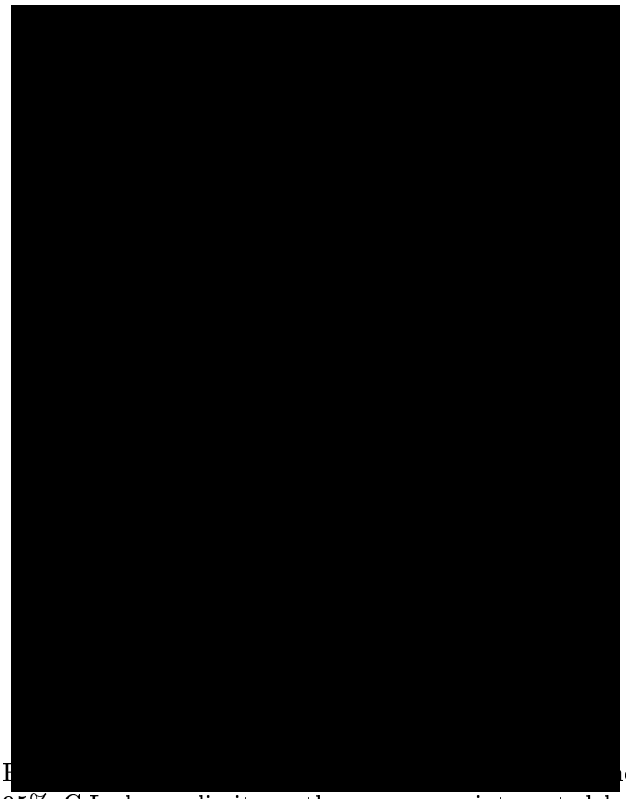

95% C.L. lower limit on the mass vs. integrated luminosity at the Tevatron for searches for new gauge bosons. The potential to discover increasingly heavy objects grows only logarithmicly with luminosity.

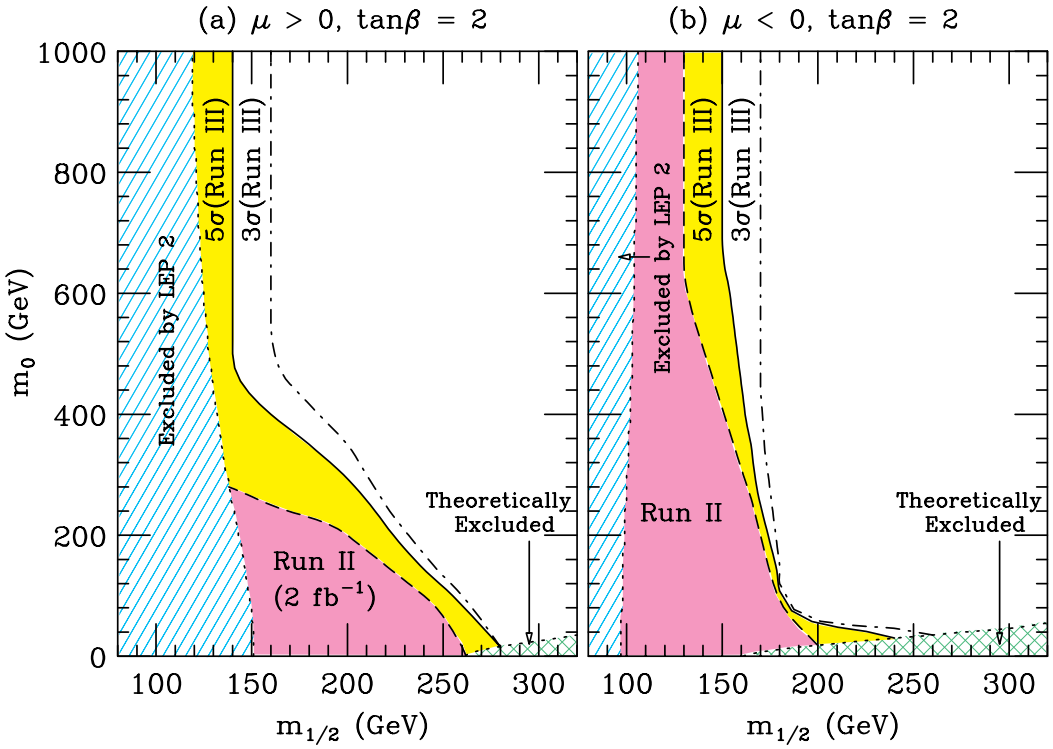


Figure 2.30: The contours of 99% C.L. observation at Run II and $5\sigma$ discovery as well as $3\sigma$ observation at Run III (30 fb$^{-1}$) for $p\bar{p} \to$ SUSY particles $\to 3\ell + X$ with soft lepton cuts in the $(m_{1/2}, m_0)$ plane, for $\tan\beta = 2$, (a) $\mu > 0$ and (b) $\mu < 0$. (from reference [15])

Table 2.13: SM backgrounds (fb) for low-$p_T$ trileptons as defined in reference [15] ("soft B" cuts). (adapted from [15])

| BG | $\sigma$ fb |
|---|---|
| $\ell'\nu'\ell\bar{\ell}$ | $0.45 \pm 0.003$ |
| $\ell\nu\ell\bar{\ell}$ | $0.20 \pm 0.004$ |
| $\ell\nu\tau\bar{\tau}$ | $0.36 \pm 0.008$ |
| $\tau\nu\ell\bar{\ell}$ | $0.13 \pm 0.008$ |
| $\ell\ell\tau\bar{\tau}$ | $0.06 \pm 0.001$ |
| $t\bar{t}$ | $0.06 \pm 0.004$ |
| *total* | 1.26 |
| 99% C.L.(2 fb$^{-1}$) | 2.5 |
| $3\sigma$(2 fb$^{-1}$) | 2.38 |
| $3\sigma$(15 fb$^{-1}$) | 0.87 |

efficiency.

Certain aspects of the Run IIb upgrade are needed to maintain CDF's excellent performance in the high luminosity environment. Precision tracking is clearly critical, not only for lepton detection and photon discrimination, but for identification of primary and secondary vertices. Thus the silicon detector, which will discriminate between multiple primary vertices along the interaction region, and detect secondary vertices with high efficiency and precision, is essential for the exotics program. In addition, the 'projective' modification of the inner layers of the COT will allow for continued high-efficiency tracking in the central rapidity ($|\eta| < 2$) region. Of critical importance is the ability to trigger on muons. This capability depends on scintillator timing in addition to stub finding in the muon drift chambers. In the intermediate rapidity range, this timing is provided by the CSX scintillators. These counters will need to be replaced for the high-luminosity run.

Several of the proposed upgrades will significantly enhance the performance of the detector for Run IIb in ways highly relevant to exotic searches. The addition of stereo information to the Level 1 trigger will have a major impact on signatures with multiple, low-*pt* leptons or displaced vertices. The additional Z information should significantly reduce fake rates. In addition, because Level 1 tracks are available for the Level 2 decision, this upgrade will allow for enhanced Level 2 track-based triggers, for example one based on a multi-track mass. This is illustrated in Figure 2.31 for the dimuon J/$\psi$ trigger. In this case the additional stereo information allows the application of a mass cut which dramatically reduces the trigger rate. Stereo tracking at the trigger level will also impact the Level 1 track trigger (Track Trigger module) which is primarily aimed at selecting hadronic decays of B hadrons. Currently this module looks for pairs of tracks. We are proposing an upgrade to the Track Trigger module that will additionally trigger on three tracks. This upgrade is primarily designed to maintain the capability for triggering on displaced vertices in a high luminosity environment.

The proposal to add timing information to the readout of the central and plug Electromagnetic calorimeters will significantly enhance our capability to do physics with photons. This timing information will already be available for the hadron calorimeters in Run IIa (central hadronic timing was available in Run I); it is critical in removing noise hits as well as identifying cosmic rays. However, the hadron timing is obviously ill-suited for the timing of electromagnetic particles. In current searches for extremely rare events, cosmic ray backgrounds remain a problem. Additionally, the timing will ensure that all photons are from the primary interaction. This will be essential at high luminosity with multiple interactions (mean $\sim 5$) per crossing. This situation is illustrated by the $ee\gamma\gamma\not\!\!E_T$ candidate event, where the hadron calorimetry timing was available for one electron and one photon in the event (see Figure 2.32). [20] In this case, both electron and photon are both consistent with the (unoptimized) 4 ns resolution. The cosmic rays background, uniform in time, is also shown. However, no timing information is available for the plug electron candidate or the second photon. The instrumentation of the electromagnetic calorimetry with timing both for central and plug calorimeters will allow timing for all electromagnetic clusters. Additionally, a 1 ns resolution is achievable with calibration. This capability would allow for searches of long-lived particles predicted in some models of gauge-mediated supersymmetry decaying to photons.

### 2.5.3 Illustrative signatures in specific models

Beginning with the Tev-2000 Workshop in 1996 [21] and continuing through the more recent Physics at Run II set of workshops sponsored by Fermilab[14], a great deal of effort has gone into studying the physics